ARL-TR-8599 ● Dec 2018

US Army Research Laboratory

Effective Coating of Planar and High Aspect Ratio Microstructure Technology (HARMST) Surfaces for a Tritiated Nitroxide Betavoltaic Nuclear Battery: the Effects of Crystallization Rates

by Johnny Russo, Hakan Berk, and David Bigio

NOTICES

Disclaimers

ARL-TR-8599 ● DEC 2018

US Army Research Laboratory

Effective Coating of Planar and High Aspect Ratio Microstructure Technology (HARMST) Surfaces for a Tritiated Nitroxide Betavoltaic Nuclear Battery: the Effects of Crystallization Rates

by Johnny Russo
Sensors and Electron Devices Directorate

Hakan Berk and David Bigio
University of Maryland, College Park, MD

REPORT DOCUMENTATION PAGE

Form Approved
OMB No. 0704-0188

1. REPORT DATE *(DD-MM-YYYY)* December 2018	**2. REPORT TYPE** Technical Report	**3. DATES COVERED (From - To)** June 2018–November 2018

4. TITLE AND SUBTITLE
Effective Coating of Planar and High Aspect Ratio Microstructure Technology (HARMST) Surfaces for a Tritiated Nitroxide Betavoltaic Nuclear Battery: the Effects of Crystallization Rates

5a. CONTRACT NUMBER

5b. GRANT NUMBER

5c. PROGRAM ELEMENT NUMBER

6. AUTHOR(S)
Johnny Russo, Hakan Berk, and David Bigio

5d. PROJECT NUMBER

5e. TASK NUMBER

5f. WORK UNIT NUMBER

7. PERFORMING ORGANIZATION NAME(S) AND ADDRESS(ES)
US Army Research Laboratory
Sensors and Electron Devices Directorate (ATTN: RDRL-SED-E)
2800 Powder Mill Road
Adelphi, MD 20783-1138

8. PERFORMING ORGANIZATION REPORT NUMBER
ARL-TR-8599

9. SPONSORING/MONITORING AGENCY NAME(S) AND ADDRESS(ES)

10. SPONSOR/MONITOR'S ACRONYM(S)

11. SPONSOR/MONITOR'S REPORT NUMBER(S)

12. DISTRIBUTION/AVAILABILITY STATEMENT
Approved for public release; distribution is unlimited.

13. SUPPLEMENTARY NOTES

14. ABSTRACT

Tritiated nitroxide has the capability to surpass all metal tritides as the viable tritium liquid and solid for a nuclear battery. Its specific activity and surface power density are potentially higher than titanium tritide. Tritiated nitroxide's other advantages over metal tritides are its various physical states and dissolvability in various common solvents. These advantages led us to the development of a simple deposition procedure when assembling a tritiated nitroxide nuclear battery prototype. The prototype results made it apparent that more investigation was required for further improvement. Thus, the goal of this research was to identify the solvent type and solute concentration (wt/wt %) that produces the thinnest and most uniform coating on planar and high aspect ratio microstructure technology (HARMST) surfaces. Through non-contact methods, a methyl ethyl ketone solution with a solute wt/wt % of 14% produced the uniform coating with a majority of its thickness being within the theoretical optimal thickness range. Results proved that coating was able to fill in approximately 98% of the surface. The compound crystal uniformity was nearly identical with two different surfaces: Si rectangular pillar array and uGaN ridge array. There was continuity with all non-contact methods used: optical profilometer, microscope camera, and MATLAB video content analysis.

15. SUBJECT TERMS
HARMST, nitroxide, tritium, profilometer, surface topography, 4H-SiC, uGaN, deposition

16. SECURITY CLASSIFICATION OF:			**17. LIMITATION OF ABSTRACT**	**18. NUMBER OF PAGES**	**19a. NAME OF RESPONSIBLE PERSON** John Russo
a. REPORT Unclassified	**b. ABSTRACT** Unclassified	**c. THIS PAGE** Unclassified	UU	65	**19b. TELEPHONE NUMBER (Include area code)** 301-394-5530

Standard Form 298 (Rev. 8/98)
Prescribed by ANSI Std. Z39.18

Contents

List of Figures

List of Tables

1. Introduction

Unattended terrestrial and low earth orbital (LEO) sensors are a growing interest for several private, commercial, and military applications. These sensors need to be low volume and weight while being continuously on for more than 5 years. Chemical-based power sources are short-term solutions and cannot sustain continuous power output of milliwatts without requiring a volume larger than the sensor itself. Nuclear batteries, also called radioisotope power sources (RPSs), provide a continuous amount of power over a significantly longer lifetime than chemical-based power sources, especially when compared to a single charge/discharge cycle. Radioisotopes have energy densities several orders of magnitude higher than chemical-based sources.[1] There is a chemical limit at an energy density of less than 10^5 J/g; radioisotopes and isomers have macroscopic intrinsic energy density between 10^8 to 10^9 J/g.[2] For most sensors, tritium ($^3H_2$) is the radioisotope of choice for RPSs because it is the least expensive beta-emitting radioisotope, has the lowest bio-toxicity, is a low-energy beta emitter, and has a half-life of 12.32 years.[3]

Tritium is a gas at standard temperature and pressure (STP) and standard ambient temperature and pressure (SATP) and must be physically contained in a vessel or chemically bonded to another compound. The state-of-the-art approach is to store tritium in metal foils forming a metal tritide.[4,5] Loading tritium into the metal crystal lattice can require extremely high temperatures and pressures.[6] Before tritiation, metal films can be sputtered directly on the semiconductor surface. A major disadvantage of this solid form is the metal crystal lattice expansion or swelling from tritium loading, thus generating internal stresses and microcracking, which worsens with helium-3 microbubble growth from beta decay. Tensile and compressive stresses develop at the interface between the foil or film and clean substrate or semiconductor diode surface because of thermal expansion mismatching. The internal and external stresses lead to foil delamination and bulking along with tritium leakage.[7] The film debonding and flaking is common when they are fully loaded (Ti^3H_2). Metal powders that have already been tritiated can be prepared in a slurry and dispensed on the semiconductor using polar or non-polar solvent and a micropipette. Lee et al. state that the tritiated slurries can be coated more uniformly on high aspect ratio microstructure technologies (HARMSTs) than the metal sputtered directly on the HARMSTs surface.[6] However, titanium tritide cannot be fully tritiated (Ti^3H_2) while being completely stable with negligible tritium leakage. The maximum loading percentage is between 81% to 85% ($Ti^3H_{1.6}$ to $Ti^3H_{1.7}$)[6,8] and 65% ($Ti^3H_{1.3}$) for powders.[6]

We have identified and developed a tritiated 6-membered and 5-membered nitroxide, which have the potential to surpass the current specific activity and β^--flux surface power density limits of metal tritides (P_{β^-}).[9,10] The two tritiation experiments provided evidence of precursor synthesis and one-step tritiation, high yield and purity, and stability in solution, oil, and solid (powder) form well above tritiated polymer previous limits. The liquid form with a solvent can be a solution, suspension, or supernate and precipitate mixture depending on solute concentration. In this report, an approach to deposit 5-membered nitroxide (C2) precursor on planar and HARMST surfaces was performed. The simple deposition procedure involved a solvent and micropipette, with which the liquid mixture was dispensed on different surfaces. A parametric study based on different solute weight concentration, solvent type, and surface type was performed. The figures of merit were the coating thickness uniformity and crystal and grain size and uniformity.

2. Solvents for Tritiated Nitroxide Dispensing

The hydrogenated, deuterated, and tritiated 5-membered nitroxides are all yellowish powder when pure and an oil when not pure (Fig. 1). The 5-membered nitroxide oil mimics the appearance and viscosity of olive oil, whereas the hydrogenated, deuterated, and tritiated 6-membered nitroxides are red-orange powder when pure and an oil when not pure. To deposit uniformly and efficiently on any type of transducer and its surface, a solvent is required to dissolve the nitroxide (powder or oil form) before the dispensing procedure is initiated. Methanol was the original solvent used for all previous tritiated nitroxide experiments. The solvent was chosen by ViTrax's head radiochemist, Dr Robert Fazio, without much discussion or analysis on the coating formation properties after the dispensing procedure. All that was known at that time was that all forms of the 5-membered nitroxide (i.e., hydrogenated, deuterated, and tritiated forms) were soluble in methanol, producing a solution. During the 2017 tritiated nitroxide (Compound 2 [C2]) and betavoltaic nuclear battery demonstration, we were not sure if all of the methanol evaporated out or was trapped within the C2 oil. The C2 droplet did not drastically reduce in volume from visible observation. This factor along with others reduced the surface power density and maximum power point (MPP) of the nuclear battery prototype.[10] We decided that more discussion, attention, and analysis on solvent selection was necessary for two main reasons. The first reason is to produce a higher power tritiated nitroxide nuclear battery with uniform and thin C2 coatings equaling the optimal layer thickness identified in our numerical models.[10] The second reason is to develop an efficient manufacturing process for C2 residue amount in dispensing tips so betavoltaic cell stacking and assembly time configuration time can be minimized.

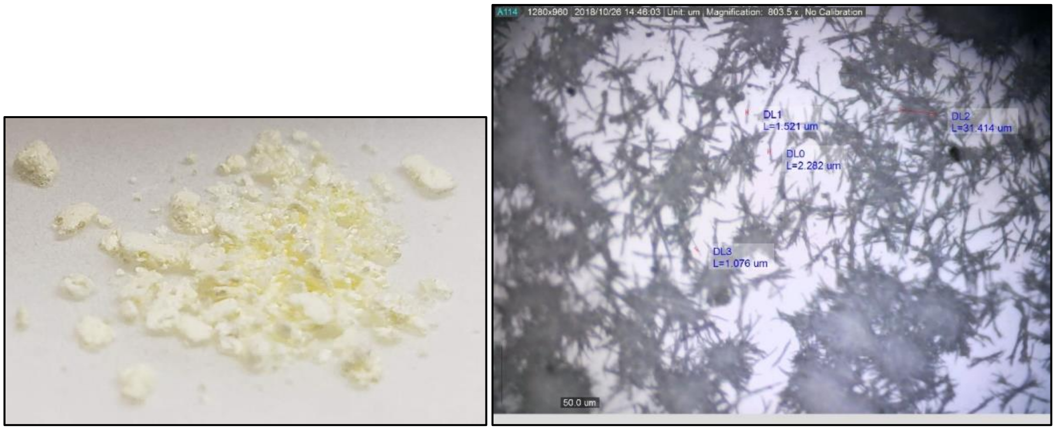

(a) (b)

Fig. 1 Images of the 5-membered ring nitroxide (C2 precursor) used in the depositing experiments: a) 5-membered nitroxide powder and b) the smallest features identified with the microscope camera were needlelike crystals that were 1 to 2 µm thick with lengths ranging from a few microns to 10s of microns

Before any decisions or solvent lists were created, an open discussion with ViTrax radiochemists was required to define the safety guidelines when tritiating and dispensing an organic compound on a transducer in a fume hood at SATP. The five selected polar solvents were methanol, ethanol, dimethylformamide (DMF), glycerol, and methyl ethyl ketone (MEK). Methanol was included as a benchmark for improvement since the solution coatings were not completely uniform with gaps and large nitroxide crystals forming on the transducer surface (Fig. 2).

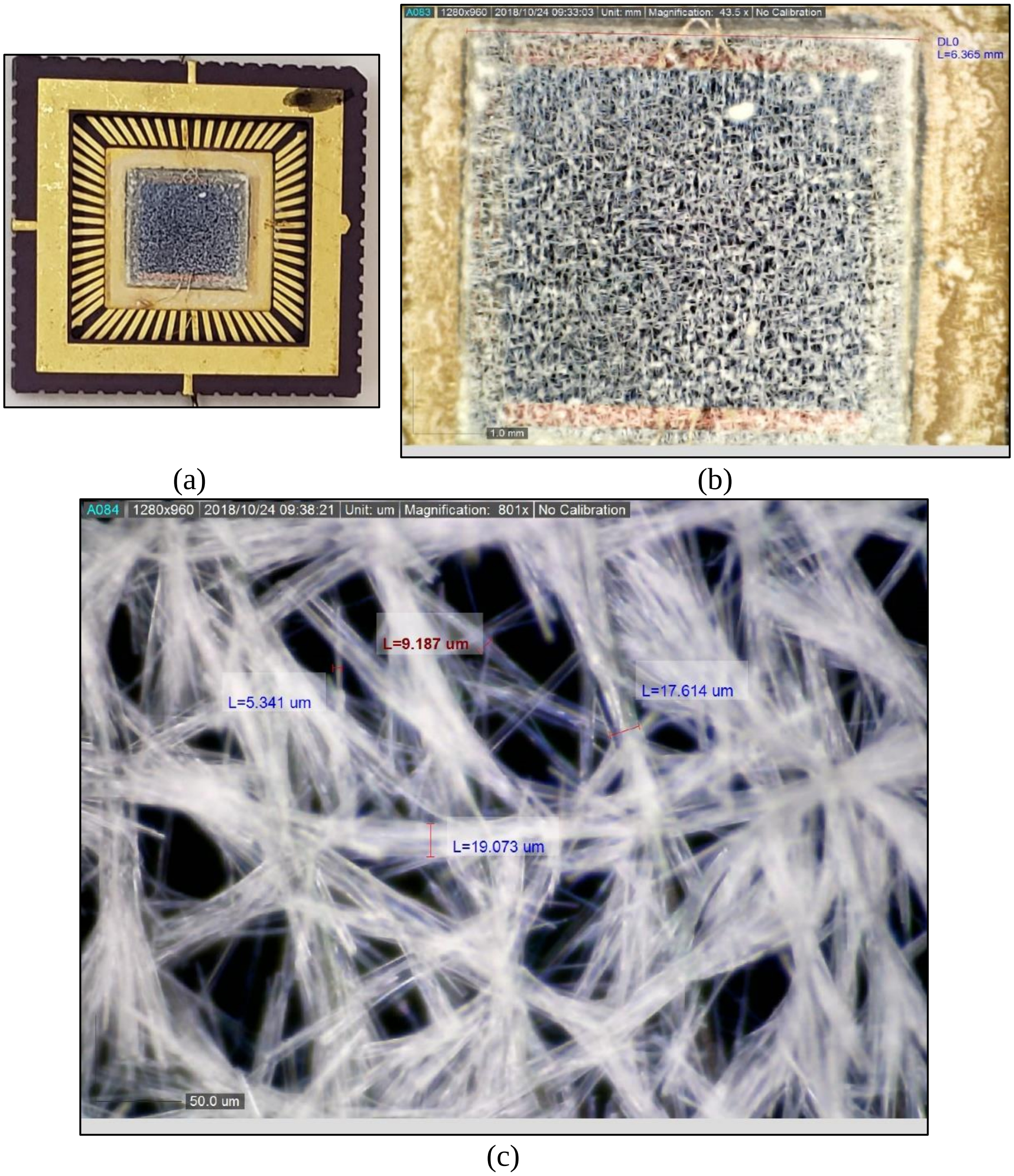

Fig. 2 Images of C2 precursor (solute) deposited on MicroLink InGaP PV cells using methanol as the solvent (a, b, and c). The solute weight percentage (wt/wt %) was approximately 6 wt/wt %. The coating clearly shown in images (b) and (c) displays noncontinuous coating with large needlelike crystal features that are more than a few microns thick/wide while being 100s of microns long.

Water was rejected from the list for three main reasons. The first and most important reason is safety and health concerns. Tritium is a major health hazard if it is taken into the body, especially in the form of tritiated water. If tritium is released from a compound, in most cases, the tritium immediately floats upward similar to hydrogen. However, if water is used as the solvent, there is not a guarantee that there will not be tritiated water formation. Tritiated water will then be absorbed, inhaled, or ingested in and travel throughout the body similar to normal water, thus increasing biological half-life of the radioisotope and increasing the short- and long-term damage of the living host.[11] The second reason is the low solubility of the C2 precursor and tritiated product with water. The solute and solvent mixture forms a suspension rather than a solution. Typically, the coatings from these suspensions are not uniform and thin, but sparse coatings with tall (hundreds of microns) features of undissolved nitroxide crystals and gaps where no nitroxide crystallization occurred. The third reason is water's intrinsic properties. Water has a higher boiling point than most solvents used in these dispensing experiments. The higher boiling point increases the evaporation time, directly increasing the nuclear battery assembly time based on the stacking configuration technique.[10] Additional heat would need to be applied on the suspension once dispensed, which increases the complexity of the procedure. Finally, this increases safety concerns since the potting and sealing steps would be postponed until the water is fully evaporated. Tritium gas loss could occur during this postponement, putting personnel at risk while reducing the power of the prototype. Water is more conductive than all selected solvents. If additional shunt resistance is introduced in the semiconductor transducer device because the water did not fully evaporate, the prototype's MPP reduces, which was observed in a previous experiment.[10]

3. Experimental Setup

The dispensing experiment comprised three major experimental setups. The first experimental setup involved the dissolution of the C2 precursor (solute) in the solvent using a micropipette, vials, and vortex agitator (also called a vortex analog mixer). Three mixtures at different solute concentrations were made for each solvent. More specifically, two solutions and one suspension mixture were made for each solvent to compare and observe the differences between the rate of evaporation, coating/crystal uniformity, crystal size, and surface spreading at a constant volume. The second experimental setup involves the dispensing of mixtures (two solution and one suspensions) on planar surfaces with and without a reservoir. The planar surface is a silicon wafer. The third experimental setup involves the dispensing of mixtures (solution and suspensions) on HARMSTs. The two different HARMST types are a silicon (Si) rectangular micropillar array with a SiO_2 top layer from Widetronix, Inc. and undoped GaN (uGaN) ridges/trenches from the State University of New York (SUNY).

3.1 Planar Setup

For the dispensing setup with planar surfaces (with and without reservoirs), two optical microscope cameras and a 15× macro lens camera were used to record dispensing of each mixture (Fig. 3). One microscope camera was positioned at 90° with respect to the surface and would provide the top view. The top view would be processed by MATLAB in order to discern information such as crystal uniformity, crystal size, and crystallization surface area (Fig. 4a). The other microscope camera was positioned at 0° with respect to the surface to capture a side view. The side view would be used to get the contact angle of the droplet with respect to the surface (Fig. 4b). A 15× macro lens camera was used to record a ~45° viewpoint, but that angle was not analyzed (Fig. 4c). Its purpose was to provide another perspective of the C2 precursor crystallization.

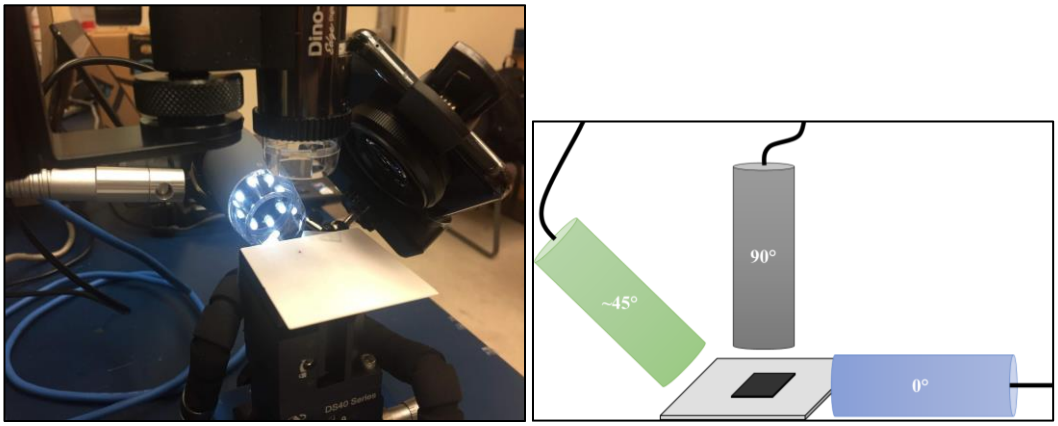

(a) (b)

Fig. 3 Experimental setup for observing C2 precursor deposition on planar surfaces: a) image and b) illustration

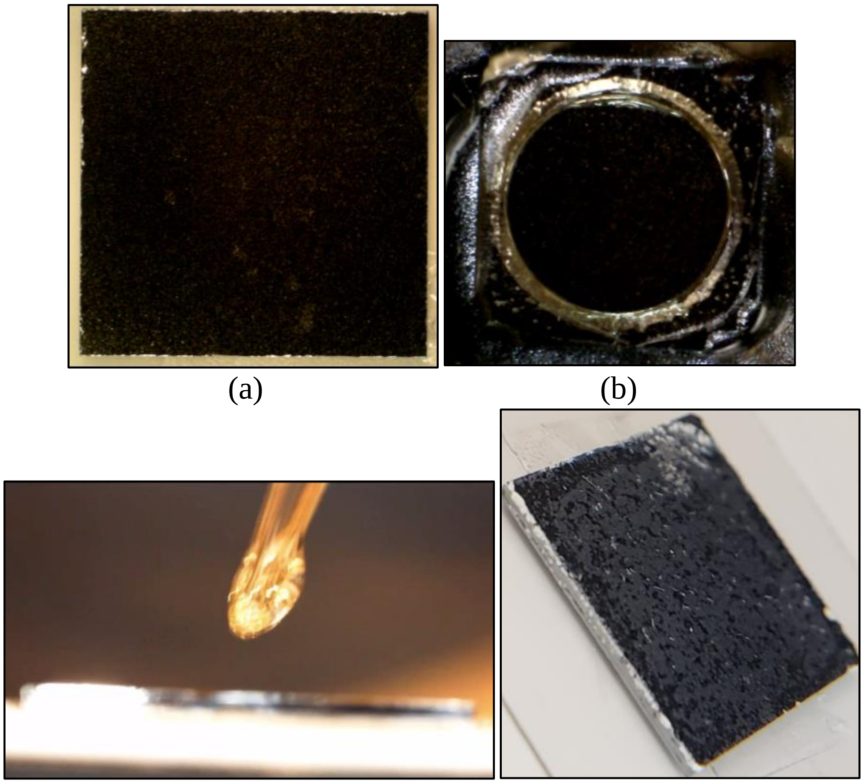

(a) (b)

(c) (d)

Fig. 4 Images of different microscope views of the planar setup: a) top view without an SU-8 reservoir, b) top view with an SU-8 reservoir, c) side view for contact angle measurement, and d) ~45° view

The purpose of dispensing C2 on a planar surface without a reservoir was to analyze the coating without an area constraint. The coating analysis comprises the contact angle measurement from the 0° positioned microscope camera, total surface area of the coating calculated by MATLAB video content analysis (VCA), and coating layer thickness measured by an optical surface profilometer. For the C2 dispensing with a reservoir, the coating analysis comprises the crystal uniformity measurement using the MATLAB VCA and coating thickness measurement with an optical surface profilometer. The SU-8 photoresist reservoirs were adhered to the Si surfaces using a UV curable epoxy. The reservoir dimensions are 510 µm by 9 mm (thickness by inner diameter) with an outer diameter of 10.2 mm. Finally, the rate of evaporation was measured for all dispensing C2 on planar surfaces, with and without reservoirs.

3.2 HARMST Setup

The HARMST dispensing setup involved a single Leica optical microscope with a microscope camera for imaging and recording during and after the dispensing of

C2. The first HARMST array was the Si rectangular micropillar array from Widetronix, Inc. (Fig. 5). The rectangular pillars were etched approximately 10.8 µm deep (***d***) with 27 nm of deposited SiO_2. The side dimensions (length by width, ***w***) were approximately 5 µm by 5 µm (Fig. 6). The feature spacing (***a***) was 5 µm, too (Fig. 7). Advanced silicon etching (ASE) was implemented to create these HARMST features. Borosilicate reservoirs were placed and adhered around the HARMST array and the planar device on the Si test wafer using the same UV curable epoxy for the planar setup. The reservoir dimensions are 500 µm and 3.2 mm (thickness and inner diameter) with an outer diameter of 4.2 mm. The surrounding surface between the reservoir and HARMST array was planar, shown in Fig. 8.

Fig. 5 Image of the Si rectangular pillar array test wafer from Widetronix. Borosilicate reservoirs were adhered to the wafer surface.

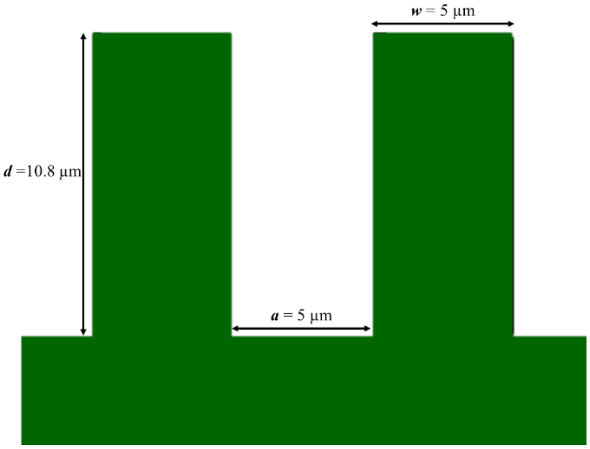

Fig. 6 Illustration of Si rectangular pillar array cross section

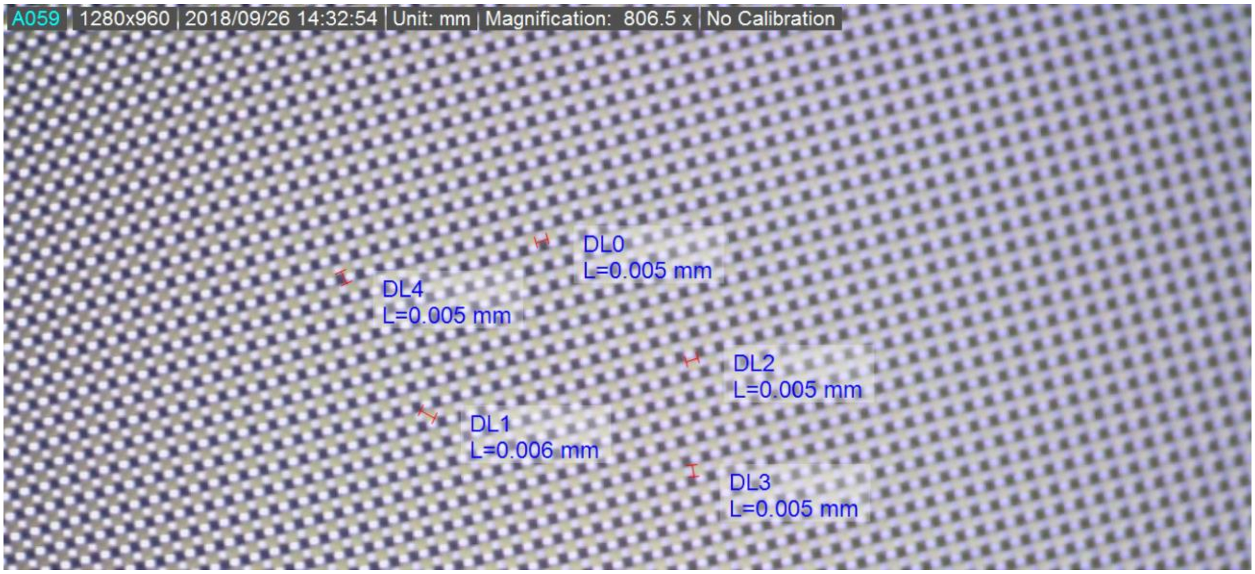

Fig. 7 806.5× magnified image of Si rectangular pillar array using the microscope camera position at the 90° in reference to the surface

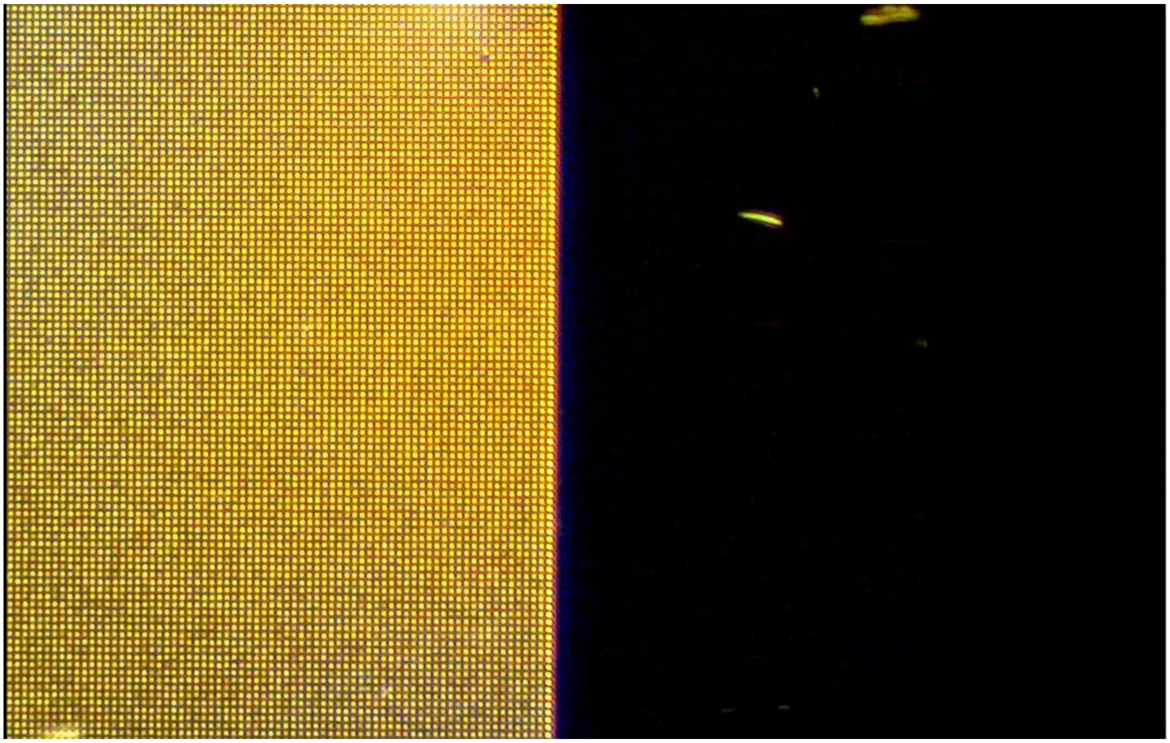

Fig. 8 Microscope view of the Si rectangular pillar array (left, yellow) and planar surface (right, black)

The second HARMST array was a SUNY uGaN ridge array at different feature spacing (i.e., *a* = 20, 25, and 30 µm) (Fig. 9). The ridges were approximately 1.5 µm tall (***d***) with a feature width (***w***) of 15 µm (Fig. 10). Deep reactive-ion etching

(DRIE) was implemented to create these HARMST features. Reservoirs were not used because the HARMST arrays were too close together.

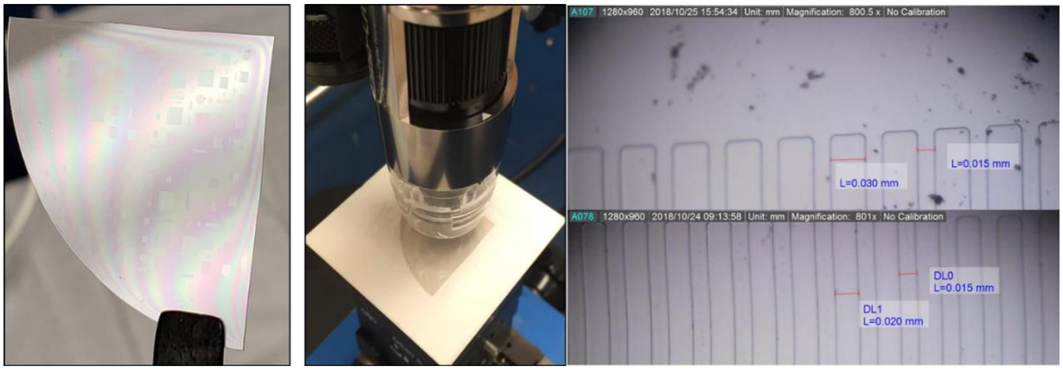

Fig. 9 Images of the SUNY uGaN HARMST wafer and planar setup

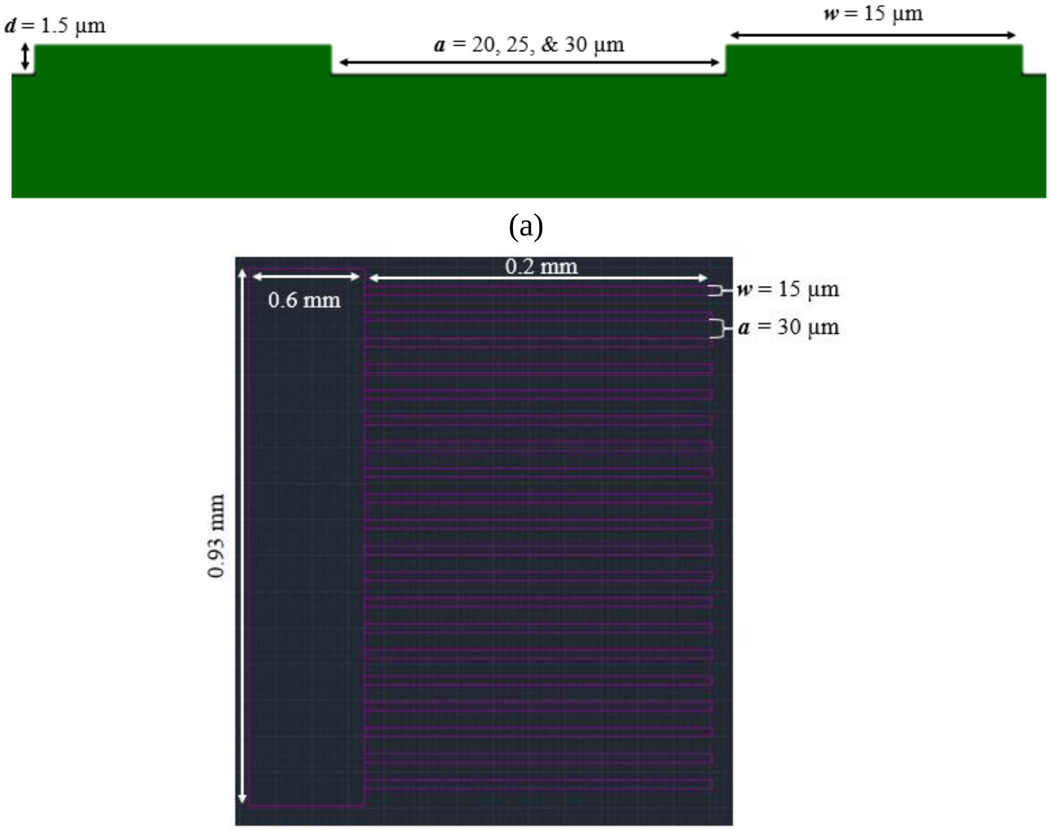

(a)

(b)

Fig. 10 a) Illustration of the uGaN ridge array cross section and b) CAD mask of one type of uGaN ridge array

4. Solute Concentrations

Three different wt/wt % mixtures were made for methanol, ethanol, and MEK. The solute was weighed and then added to the vial before solvent dispensing. To accurately identify when the solute fully dissolved (solution) or began forming into a suspension, the solvent was added at 1 µL intervals and briefly hand-stirred or stirred using the vortex analog mixer. For DMF, only one type of solute concentration solution was made because the solution droplet produced a contact angle where it did not dry down to a thin coating like the other mixture droplets. This is explained in Section 5. The dissolution and dispensing with glycerol was unsuccessfully attempted because the viscosity was too high. The mixing and dispensing procedure would have to be completely altered to utilize glycerol effectively. Two solutions and one suspension were made for the other solvents, excluding DMF and glycerol. One of the solutions for each solvent was approximately 6 wt/wt %, producing a yellow solution with all three solvents. The other solution was at different wt/wt % for each solvent at the point where complete dissolution of the solute occurs after using the vortex analog mixer for a few minutes. The last mixture was a suspension at different wt/wt % for each solvent at the point where the solute is still suspended in the mixture. The solute wt/wt % and solvent of each mixture is listed in Table 1.

Table 1 Name, solute wt/wt%, and solvent and mixture type for each mixture used in this deposition experiment

Mixture name	Solvent type	Solute wt/wt %	Mixture type
s1v1	Methanol	6.3	Solution
s1v2	Methanol	8.0	Solution
s1v3	Methanol	13	Suspension
s2v1	Ethanol	6.0	Solution
s2v2	Ethanol	7.1	Suspension
s2v3	Ethanol	3.6	Solution
s3v1	DMF	7.5	Solution
s5v1	MEK	5.9	Solution
s5v2	MEK	14	Solution
s5v3	MEK	17	Suspension

5. Contact Angle Measurements

5.1 Introduction

An important factor in determining the best mixture for the nitroxide is the contact angle between the droplet and surface, planar or HARMST. The contact angle is observed and measured with the optical microscope camera positioned at 0° for planar surfaces (Fig. 3b). The goal is for the compound to spread across the surface rather than beading up in the center and eventually evaporating out. Obtaining this result would involve the droplet spreading immediately as it is dispensed on the planar surface. Therefore, the best result would be if a contact angle is not able to be measured, in other words, a contact angle of approximately zero. Since the droplet volume of 2 µL is constant for each sample, those with the smallest contact angle would have the largest surface area of spreading on the planar surface. If a contact angle is able to be measured, the smallest angle would be desirable just as the largest surface area is desirable.

5.2 Results

Four of the five solvents were used in the contact angle measurements. Methanol, ethanol, DMF, and MEK were analyzed. Glycerol's viscosity is too high, preventing solute and solvent mixing and the droplet dispensing. Methanol, ethanol, and MEK achieved the desired result of having a contact angle of 0°. DMF was the only compound to make a bead when dropped on the surface, and thus the only compound whose contact angle could be measured. Three samples of DMF at the same solute wt/wt % were used to get multiple measurements of the contact angle.

Images were taken using the microscope cameras after the droplet had settled (Fig. 11). These images were then loaded into ImageJ in order to measure the contact angle. For each droplet, an angle was taken from the left side and right side of the droplet. This approach was used to conform the level of axial symmetry of the droplet (Fig. 12). Since using ImageJ to measure the contact angle is not the most accurate method, a degree or two of difference between the left and right side of the same droplet is determined not to be significant. In fact, only one droplet had the same measurement for the left and right side, shown in Table 2.

Fig. 11 2-µL droplet of s3v1 on a Si planar surface. The DMG, solvent, did not evaporate during the microscope video recording. Instead, it formed a hard shell made up of the dried solute (C2), trapping the solvent inside the shell. The contact angle of the droplet was not axially symmetric.

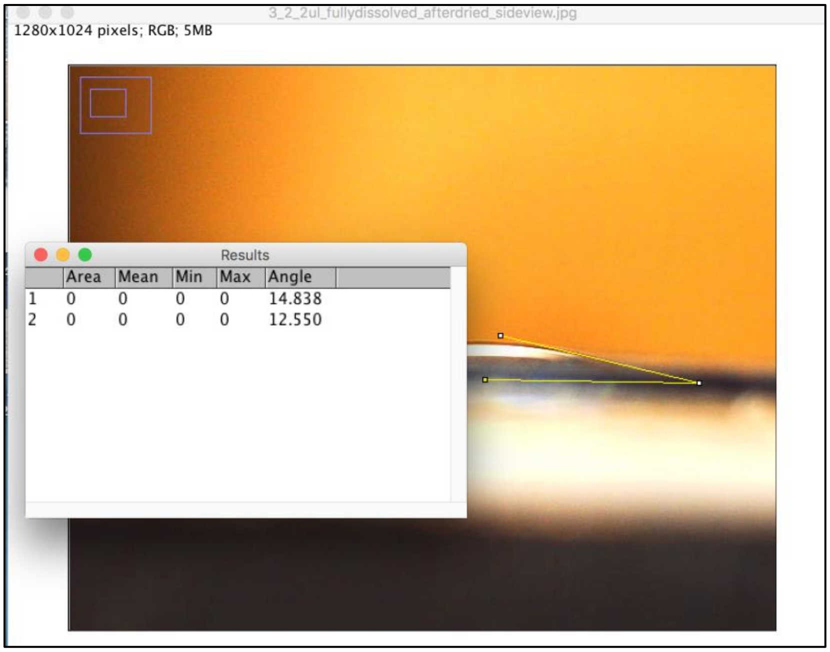

	Area	Mean	Min	Max	Angle
1	0	0	0	0	14.838
2	0	0	0	0	12.550

Fig. 12 ImageJ contact angle measurement view for 2 µL droplet of s3v1 on a Si planar surface

Table 2 Contact angle measurements of s3v1 droplets on Si planar surfaces

Angle measurements (°)	Mean (°)	Standard deviation (°)
19.4	16.1	3.77
14.8		
15.5		
21.8		
12.6		
12.6		

Since DMF has a contact angle measurement, it was removed from the list of possible compounds for the tritiated nitroxide nuclear battery. The angle measurements were not very consistent as each sample provided contact angles that varied by a couple degrees. Since DMF was removed, more measurements were not done for this compound since it was no longer within the scope of the research. However, if desired, more data can be collected on this as a larger number of samples is necessary to figure out the experimental mean and standard deviation values for the contact angle of the DMF compound.

6. Rate of Evaporation for Planar Surfaces

Another important factor in determining which solvent and solute wt/wt % is optimal for the tritiated nitroxide nuclear battery is the evaporative crystallization time of the mixture. This is important as a safety feature because it enforces a minimum of potential tritium gas release before potting and encapsulant epoxy is applied. This is also essential to speed up the manufacturing process of the tritiated nitroxide nuclear batteries. The evaporation time was measured and compared for different mixtures (solutions and suspensions). This measurement has a qualitative component, as the time taken for evaporative crystallization was determined by when there appeared to be an undetectable amount of change in the video of the crystallization process. The results of this can be seen in Table 3.

Table 3 Crystallization time for different mixtures deposited on Si planar surfaces

Mixture name	Solvent/mixture type	Solute wt/wt %	Mean (in seconds)	Standard deviation (seconds)	Number of samples
s1v1	Methanol / Solution	6.3	72	24	3
s1v2	Methanol / Solution	8.0	31	1.4	2
s1v3	Methanol / Suspension	13	87	86	3
s2v1	Ethanol / Solution	6	47	13	7
s2v2	Ethanol / Suspension	7.1	94	8.4	7
s2v3	Ethanol / Solution	3.6	26	5.2	3
s3v1	DMF / Solution	7.5	∞	∞	3
s5v1	MEK / Solution	5.9	59	23	3
s5v2	MEK / Solution	14	15	1.7	3
s5v3	MEK / Suspension	17	42	12	3

The first column of Table 3 indicates the name of the sample that was used. Four of the five original compounds were used for this experiment. Since DMF did not evaporate or spread, it was not tested with the reservoir, or the suspension mixture type. The rest of the samples were tested in the planar setup along with the reservoir setup. Column 2 describes the solvent and mixture type for that specific experiment. Column 3 indicates the difference in concentration by weight percentage for each of the experiments. Column 4 indicates the average evaporation time for each of the different types of samples while Column 5 indicates the standard deviation.

The first thing that can be seen from Table 3 is that the reservoir significantly increases the time that it takes for every compound to evaporate. There are two reasons for the difference with evaporation time. First, the reservoir blocked any wind or airflow that was in the laboratory. Second, the surface area for the reservoir is much smaller than the planar region. A smaller surface area leads to a slower rate of crystallization. In addition, methanol and ethanol tend to take much longer than MEK to evaporate. Methanol-based mixtures tend to have more variance in the evaporation times, as seen with the large standard deviation. This inconsistency does not make methanol an appealing choice as the best solvent, as this would make any possible future standardized manufacturing process difficult. The combination of having similar evaporation times along with a much lower standard deviation makes ethanol a more appealing compound to use when compared to methanol. s5v2 has the lowest evaporation time and lowest standard deviation, which means it is the fastest and most consistent mixture. Just from the timings shown in Table 3, this makes MEK the best solvent when dispensed on planar surfaces with relation to evaporation. While some trends can be seen, more data would need to be taken to confirm these initial experimental results.

7. Evaporation on Planar Surfaces

The objective of this experiment was to quantify the amount that each compound spread onto the planar surface. The volume dispensed was the same for each compound: 2 µL. Therefore, the sample with the largest surface area covered would mean that it had the thinnest layering on top of the surface. The surface that each compound was being dispensed onto was the exact same, a 1 × 1 cm Si wafer. The thinnest layer provides the most benefit because it minimizes the beta energy self-absorption of the layer, so the mixture that covers the largest surface area will be the optimal choice for the tritiated nitroxide nuclear battery.

By the end of this experiment, the goal is to continue to rank the mixtures as possible candidates for the tritiated nitroxide nuclear battery. In order to do this, each of the videos of the droplet spreading on the surface have to be analyzed. This analysis is done through MATLAB because it is able to recognize objects in pictures and has tools for video content processing. The first frame would be taken as a control to be compared to the rest. Then, the control frame would be subtracted to the current frame to see the differences between the images. The difference would be the droplet spreading and the crystallization process. Then, built-in MATLAB functions could be used to count the number of different crystals, the size of the crystals, their perimeter, and their area.

One difficulty with this process is that every mixture was partially translucent. This made it much more difficult for MATLAB to discern a difference or whether or not there was liquid on the surface. Adding a dye to the compound was not an option since adding another liquid would change the properties of the droplet during dispensing. It was only after the mixture had crystallized with solvent evaporation that MATLAB could distinguish that the crystals were no longer transparent. Since not all of the mixture crystallized, the total surface area was the area of crystallization plus the rest of the surface area covered by the liquid. This discrepancy can be seen in Fig. 13 for methanol. The black areas between the crystals had liquid while the black area in the upper right was untouched and

MATLAB was unable to discern the difference. This made the process of finding the total surface area more of an estimation than an exact value.

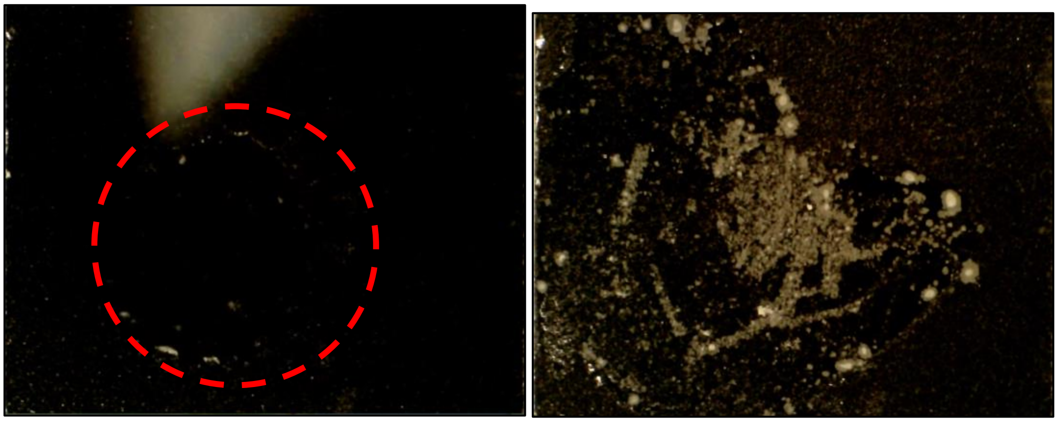
(a) (b)

Fig. 13 Microscope images of a) the initial start of solvent evaporation and b) C2 crystallization completion, using methanol as the solvent at solute wt/wt % of 6.3 (s1v1; refer to Table 1); a) shows the light coloration in the shape of the triangle with the micropipette tip exiting the camera view

7.1 Methanol

The s1v1 droplet, encircled by the red dashed line, spread out immediately as soon as it touched the surface, as seen in Fig. 13a. The outline of the droplet is not well defined, and the partially translucent solution is within that boundary. Figure 14 shows the inconsistency with samples at the same solute wt/wt %.

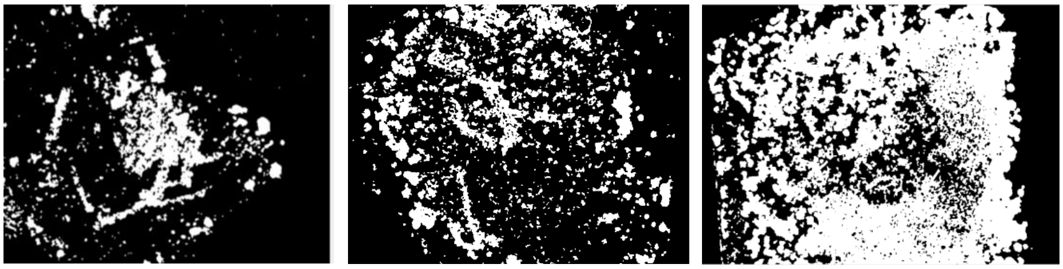
(a) (b) (c)

Fig. 14 MATLAB VCA comparison between three samples at 6.3 wt/wt % using methanol as the solvent (s1v1; refer to Table 1)

Each of the three samples of Fig. 14 had the same wt/wt % and dispensed volume of 2 µL. The inconsistency is concerning for the application of the tritiated nitroxide nuclear battery since the power output and beta efficiency will not be consistent. Therefore, it will be difficult to rate the performance of the RPS. This is further evidence that methanol is likely not the best solvent for the tritiated nitroxide nuclear battery. In addition, when dispensing on HARMST surfaces, the coating quality and result would be nearly impossible to predict because of the difference in crystal size and crystal density between each sample at the same solute concentration.

7.2 Ethanol

The s2v1 droplet, encircled by the red dashed line, had a slightly larger amount of surface tension given that it did not spread immediately, as seen in Fig. 15a. The crystallization reaction (Fig. 15b) produced larger, coarser crystals when compared to methanol or MEK. A good attribute about the crystallization is that it covered the entire surface area. This is something that no other solvent was able to do at a droplet volume of 2 µL. Some of the black background from the original surface is seen, and that is likely due to the coarser crystals not being able to fill in the entirety of the space. While the surface area coverage is excellent, the large crystals are a cause for concern. The larger the crystals are, the longer distance the beta particles will have to travel to get to the semiconductor. This will make the tritiated nitroxide nuclear battery not as efficient, as finer crystals would be more optimal, especially when attempting to fill within the microstructure gaps.

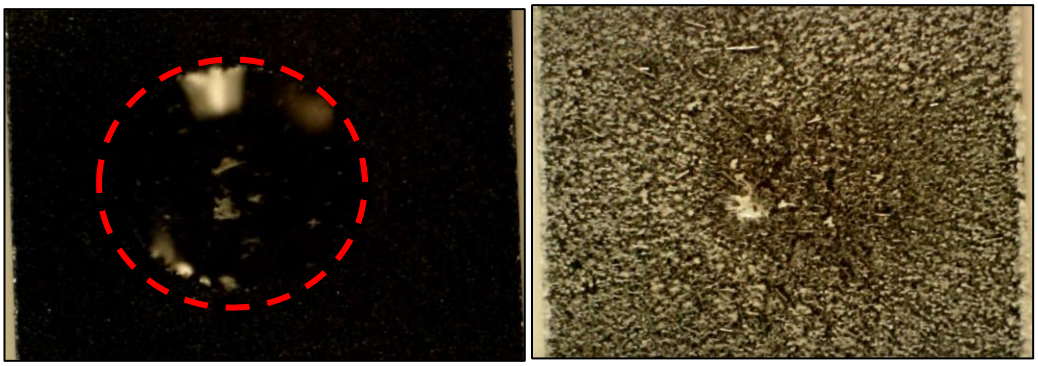
(a) (b)

Fig. 15 Microscope images of a) the initial start of solvent evaporation and b) C2 crystallization completion, using ethanol as the solvent at solute wt/wt% of 6 (s2v1; refer to Table 1)

7.3 DMF

When the other mixtures were dispensed, the droplet tended to spread immediately across the surface. The s3v1 (DMF-based solution) droplet, encircled by the red dashed line, was stationary for the entire duration and did not get any thinner from the starting point (Fig. 16). Solvent evaporation was halted because the outer coating C2 precursor hardened, trapping the solvent within the droplet ellipsoid hemisphere. This eliminates DMF as a potential solvent because this middle portion has been coated too thick and will have a lower beta efficiency than methanol,

ethanol, and MEK. In addition, the rest of this surface will not have any beta energy deposition since the droplet does not spread out any further.

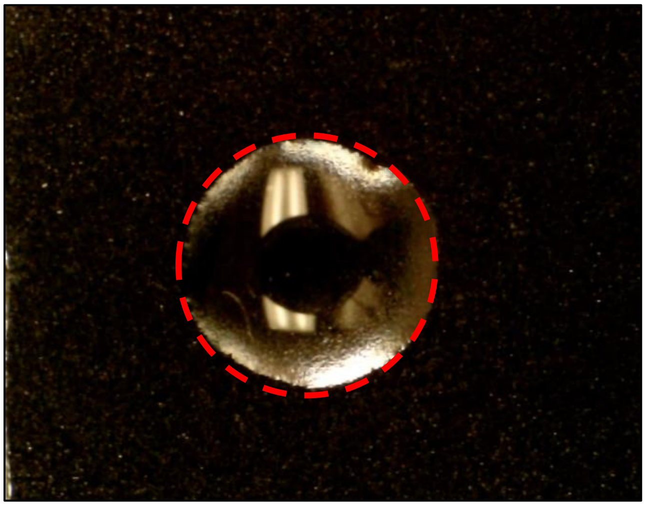

Fig. 16 Microscope images of the s3v1 droplet on the Si planar surface. The DMF did not evaporate out because of a thin C2 coating that formed over the entire droplet surface.

7.4 MEK

MEK-based solution had the largest amount of surface tension compared to the other solvents that eventually spread across the planar surface. The middle of the droplet stayed intact while a ring on the outside spread to its final boundaries within the first few seconds. The crystallization process with MEK evaporation was completed in the next 15 s as seen on the right of Fig. 17. The evaporation rate at which the MEK-based solution starts and finishes its crystallization process is faster than every other tested solvent.

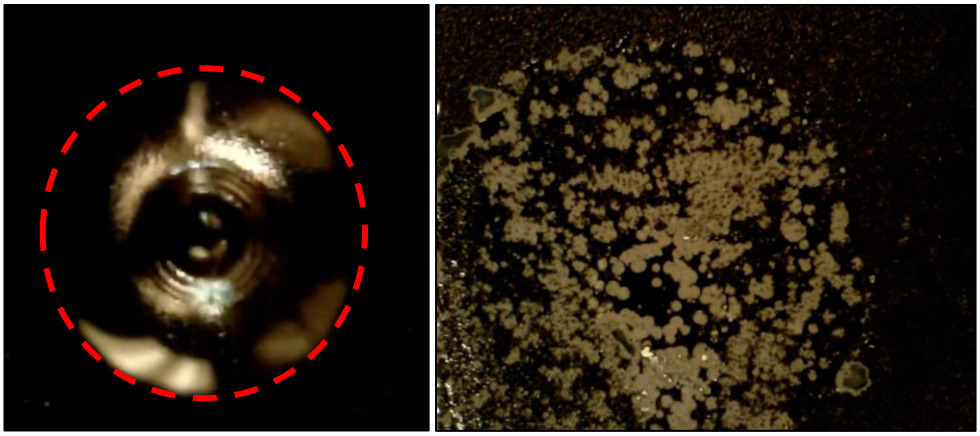

(a) (b)

Fig. 17 Microscope images of a) the initial start of solvent evaporation and b) C2 crystallization completion, using MEK as the solvent at solute wt/wt% of 14 (s5v2; refer to Table 1).

7.5 Surface Area of Various Compounds after Evaporation

As seen in the prior section, the ethanol-based mixtures covered the most surface area out of all the mixtures, making it the ideal candidate in that regard. MEK- and methanol-based mixtures covered similar amounts of surface area, while DMF-based solution did not spread at all. DMF will not be continued to be researched as a solvent option. Methanol, ethanol, and MEK will all undergo the crystal uniformity test using the SU-8 photoresist reservoirs. Finding the area of the starting region of methanol involved ascertaining the coordinates of this boundary in order to find the major and minor axis of this ellipse. Then, a conversion from pixels^2 to cm^2 is applied given the entire square is 1 cm^2 and the resolution of the video is known from MATLAB (Table 4).

Each droplet has the same volume of 2 µL, but the different solvents had different initial starting surface area measurements. Surface tension and viscosity had an important role in this variation; these two properties of each mixture were not measured but evident differences were observed. The variation occurs because there is a non-negligible amount of time it takes for the micropipette to leave the frame, as the droplets are being dropped manually. In this time, the droplet has time to spread out before an initial measurement is able to be taken. Therefore, the size of the initial measurement is dependent on the surface tension of the mixture droplet when in lands on the surface, and not when it is ejected from the micropipette.

Table 4 Initial and final surface area of mixture droplet

Mixture name	Initial surface area (cm^2) at t = 0 seconds	Final surface area (cm^2)	Area coverage % (percentage of total area)
s1v1	0.13	0.55	55%
s2v1	0.25	0.88	88%
s3v1	0.14	0.15	15%
s5v2	0.35	0.69	69%

8. Surface and Crystal Uniformity on Planar Surfaces

Another important factor for selecting the best solvent and solute wt/wt % for the tritiated nitroxide nuclear battery is to analyze and measure the surface and crystal uniformity after crystallization has completed. Surface uniformity is important because a thinner uniform coating maximizes the beta source efficiency. Crystal uniformity is an important factor because if the crystals are not uniform, they may not fit into the microstructure gaps. This experiment was done in the reservoir format, which took much longer for the crystals to form since it was a smaller surface area compared to the previous planar experiments.

8.1 Methodology

The microscope cameras recorded the crystal formation growth for each compound. The recording would start, and then the droplet was dispensed. The video recording would stop when it was determined there was no longer any crystal growth where the evaporation was completely evaporated out. Next, the microscopes zoomed in to approximately 40× and 800× magnification to see the grain feature dimensions of the crystals. Measuring the grain dimensions and shapes of the crystals is also important for determining the best solvents and concentrations to move forward with the HARMST rectangular pillar array.

The crystal formation that formed was white for every compound. This helped in the analysis because as the crystal formation forms and covers the surface, the reservoir gets more and more white. If using RGB, white is considered to be 255 for each pixel value while black is considered to be 0. Therefore, a measurement of how white a picture is would be to take the average pixel value over the entire image.

8.2 Results from MATLAB Analysis

8.2.1 Methanol

Figure 18a shows one minute after the mixture was dispensed onto the reservoir. The start of the crystallization shows that there were many individual places where crystallization started, for it did not start in one place and spread out. Figure 18b was from the last frame of the crystallization video. Those initial areas of crystallization are the brightest in the final frame. The areas in black are areas that did not crystallize.

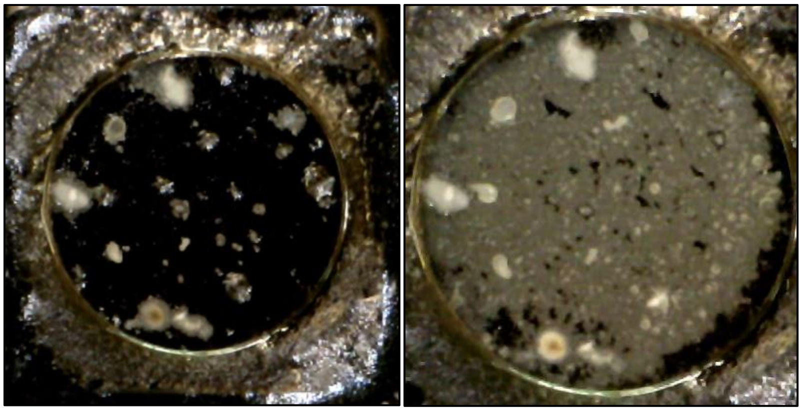
(a) (b)

Fig. 18 Microscope images of the solvent evaporation: a) after 1 min and b) after C2 crystallization completion, at a magnification of approximately 40× using methanol as the solvent at solute wt/wt% of 6.3 (s1v1; refer to Table 1)

Figure 19 represents the average pixel value for the methanol-based mixture. All graphs will have a large spike in the beginning. This spike or large peak is when the micropipette is entering or exiting the microscope camera view and dispensing the droplet into the reservoir, producing an extremely bright lighting of white. As soon as the micropipette and user’s hand are removed from the frame, the average pixel value goes down and then slowly starts increasing as the crystals are being formed. The flat portion between the large peak and second peak is the settling period of the droplet. The second peak is the initial crystallization of the solution. The small dips and valleys are the lighting changes as the liquid is crystallizing. The crystallization rate begins to increase after the initial crystallization peak. The same regions of the curve were present with the other mixture crystallization plots. The x-axis represents the current frame in the video, as the calculation for the average pixel value is done every frame to have as many data points as possible. The video being processed has a frame rate of 30 frames per second, which indicates that the time the compound took to fully crystallize was about 150 s.

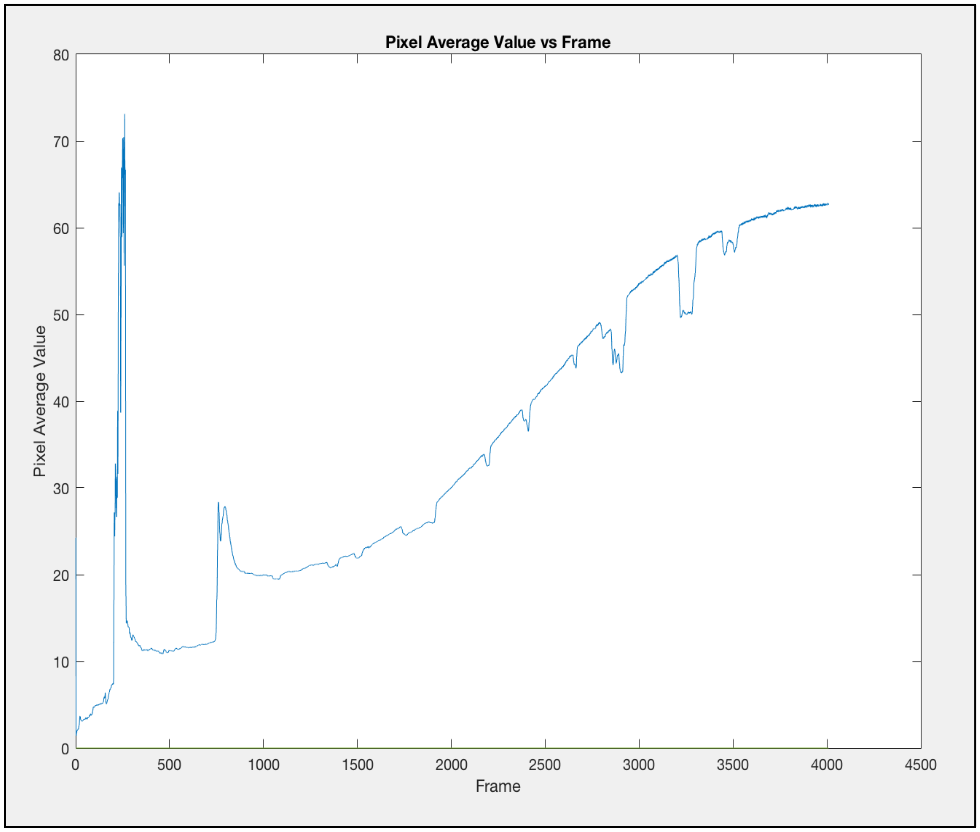

Fig. 19 The white pixel average value as a function of frames for s1v1 droplet dispensed within the SU-8 reservoir. The white pixel average value represents the C2 crystallization on top of the black background of the Si planar surface. The first peak/spike is when the micropipette enters and exits the microscope camera view. The second, large peak is the initial crystallization after the solution settling period. After the second peak, the crystallization rate increases rapidly. The small dips/valleys are the lighting changes as the liquid is crystallizing.

8.2.2 Ethanol

The second experiment was with ethanol as the solvent (Fig. 20). The large white areas are large crystals that have formed on the surface of the reservoirs. Around the edge of the reservoir, there are finer, smaller crystals. This already shows that there is a lack of uniformity with the different types of crystals that have formed. There is a large difference in the formation of the crystal formation between methanol and ethanol. When crystals formed with the methanol-based mixtures, it was uniform throughout the reservoir. When crystals formed with the ethanol-based mixtures, there were two types of crystals. The crystals on the outside edge of the reservoir started by forming finer crystals and spread inwards, while the inside, coarser crystals started in the middle and spread outwards. These different crystal formations and end sizes are detrimental for the goal of crystal and surface uniformity.

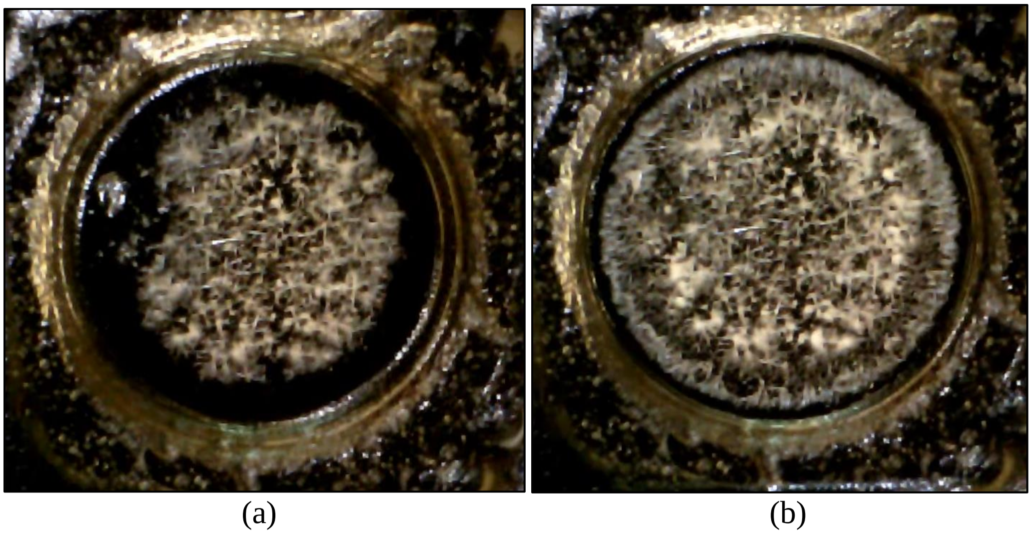
(a) (b)

Fig. 20 Microscope images of the solvent evaporation: a) after 1 min, and b) after C2 crystallization completion, at a magnification of approximately 40× using ethanol as the solvent at solute wt/wt% of 6 (s1v1; refer to Table 1)

As shown in Fig. 21 from the methanol-based mixture, there was a similar spike with the droplet being dispensed into the reservoir at around 480 frames into the video. Then, from frame 500 to about 1000 the droplet is settling in and spreading out. At frame 1000, the mixture begins to crystallize as more and more white is detected. It is important to note how the rate of crystallization is much faster, as shown through the steeper slope of pixel value when compared to the methanol-based mixtures. Also, the average pixel value at the end is significantly higher than that of the methanol-based mixture (100 vs. 60) shown in Fig. 19. Finally, the time for this crystallization was much faster, as it only took 2500 frames (or 83 s) instead of the 4500 frames (or 150 s) for the methanol-based mixture. Due to these factors, ethanol is a better solvent than methanol to use for dispensing on the HARMST arrays.

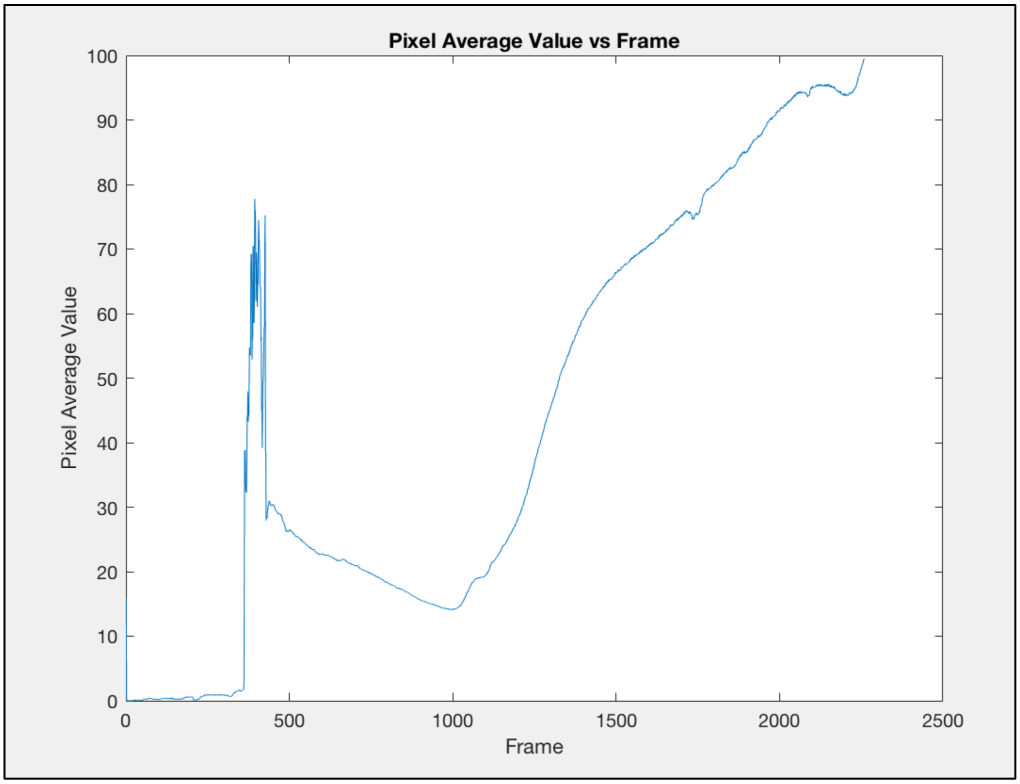

Fig. 21 The white pixel average value as a function of frames for s2v1 droplet dispensed within SU-8 reservoir

8.2.3 MEK

The MEK-based mixture varied in the way that the crystal formation formed. As seen in Fig. 22, the initial crystal formation differed immensely for these two different samples. For the sample on the left (Fig. 22a), the crystallization started in the middle, and then started branching outwards. It looked similar to the way a root system of a tree would form and branch out. For the sample shown in Fig. 22b, the crystallization started in the bottom right and top left. Then, after a short period, the different areas of crystallization began to connect. Despite the differences in the initial crystallizations, the end crystal looked nearly identical for each sample (Fig. 23).

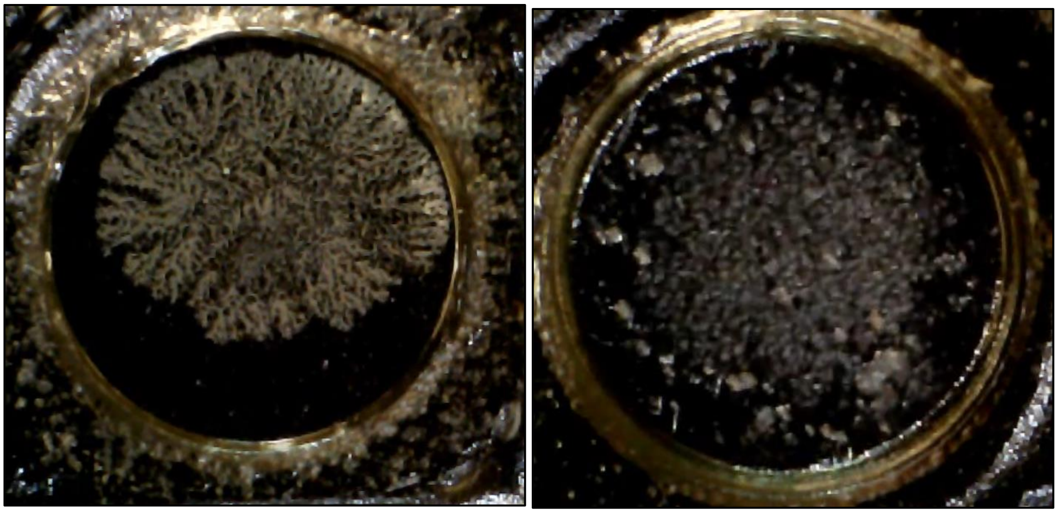

(a) (b)

Fig. 22 Microscope images of the of solvent evaporation after 1 min: a) s5v1 (5.9 wt/wt % of solute) and b) s5v2 (14 wt/wt % of solute) at a magnification of approximately 40× using MEK as the solvent (s5v1 and s5v2; refer to Table 1)

Fig. 23 Microscope image of the C2 crystallization completion of s5v2 (14 wt/wt % of solute) at a magnification of approximately 40× using MEK as the solvent

At a glance, the final crystal formation looks very fine without as many differences in crystal formation as seen in the methanol-based mixtures. In addition, there seems to be a uniform covering of the surface with finer, smaller crystals compared to the other two mixture types.

One major advantage of MEK-based mixtures was its rate of crystallization. The droplet was inserted at the spike in the graph around 220 frames or about 7 s into the video recording (Fig. 24). There were 5 s before the mixture started crystallizing when compared to both ethanol- and methanol-based mixtures. In addition, the slope at which the reservoir is becoming whiter is much steeper when compared to the other two mixture types. This demonstrates that not only did the crystallization process start quickly, it was a very rapid process to go from a liquid to covering the reservoir with crystals. Also, it is interesting to note that the MEK-based mixture reached its peak average pixel value around frame 800 and stayed steady until the end of the video around frame 1200. Therefore, the entire process from the sample being inserted to the end of crystallization changes took only 600 frames or 20 s in the reservoir. This is at least 3× as fast as the ethanol- and methanol-based mixtures. This fast evaporative crystallization speed is optimal for optimizing the manufacturing process of the nuclear battery. Finally, the average pixel value for MEK was higher than that of the other two mixture types. MEK appears the best solvent for the tritiated nitroxide nuclear battery based on the SU-8 photoresist reservoir experiments.

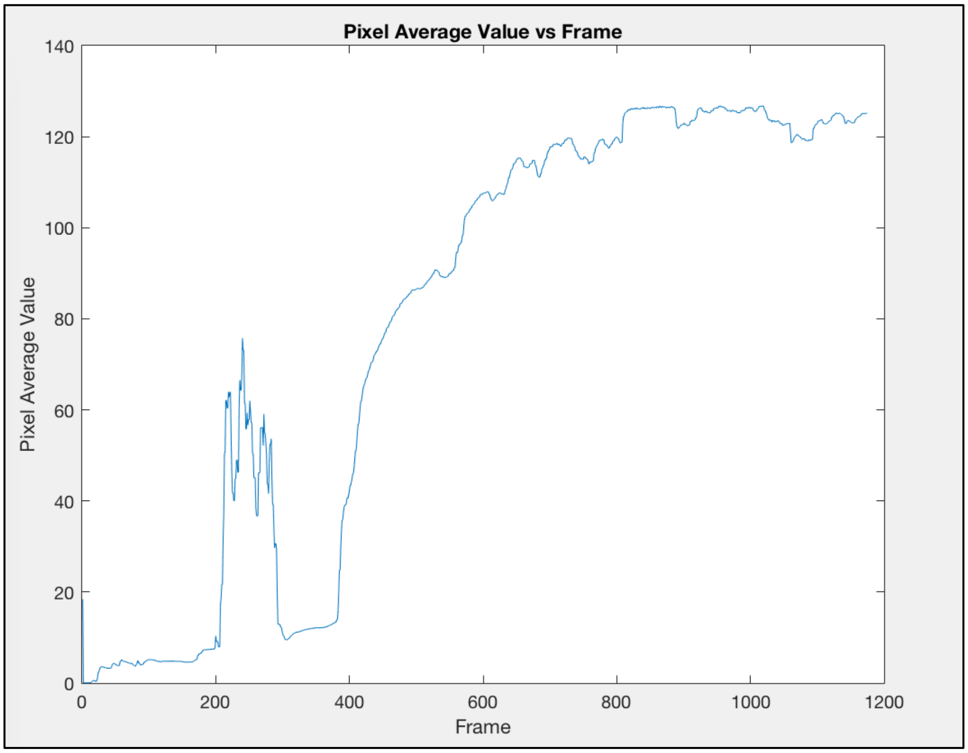

Fig. 24 The white pixel average value as a function of frames for s5v2 droplet dispensed within SU-8 reservoir

8.3 Compiled MATLAB VCA Results

Table 5 shows a qualitative result of the findings based on the videos and graphs generated by MATLAB VCA.

Table 5 Compiled results of mixture deposition in SU-9 reservoirs

Solvent type	Average pixel value	Time it takes for crystallization to begin forming	Crystallization time	Crystallization rate
Methanol	Low	Long	Long	Slow
Ethanol	Medium	Medium	Medium	Medium
MEK	High	Short	Short	Very fast

8.4 Profilometer and Microscope Measurements for 2-D Surface and Crystal Uniformity on Planar Surfaces

After the completion of the MATLAB VCA, surface uniformity, thickness, and crystal uniformity were measured by calibrated instruments. The 2-D surface uniformity and thickness are quantitative results because they can be measured across the sample's diameter. The crystal uniformity is a qualitative result because there are several different dimensions of the crystals. Based on previous observations, the crystal shapes and orientation are typically similar over the entire sample. The calibrated instruments and MATLAB will confirm the level of accuracy with MATLAB VCA results. An optical profilometer was used to measure the 2-D surface uniformity and thicknesses through laser scans across C2 coatings within the reservoir. The optical profilometer model was a Micro-Epsilon optoNCDT ILD1800-2(100). The 1-mW laser spot size was 80 µm with a wavelength of 670 nm. The samples were placed on and translated across the stationary laser beam using a Newport DS40-XYZ Compact Dovetail Linear Stage. Figure 25 shows an image of the experimental setup. Scans were done for each sample across its diameter, shown in Fig. 26. The sample points where the layer thickness is zero means that either the coating was too translucent for the profilometer to pick up a measurement or there was no C2 coating.

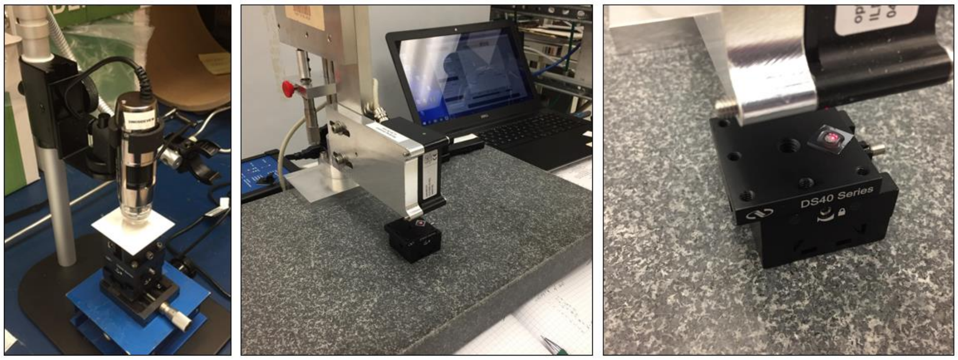

Fig. 25 Images of the microscope and optical profilometer measurement setup for planar and HARMST surfaces

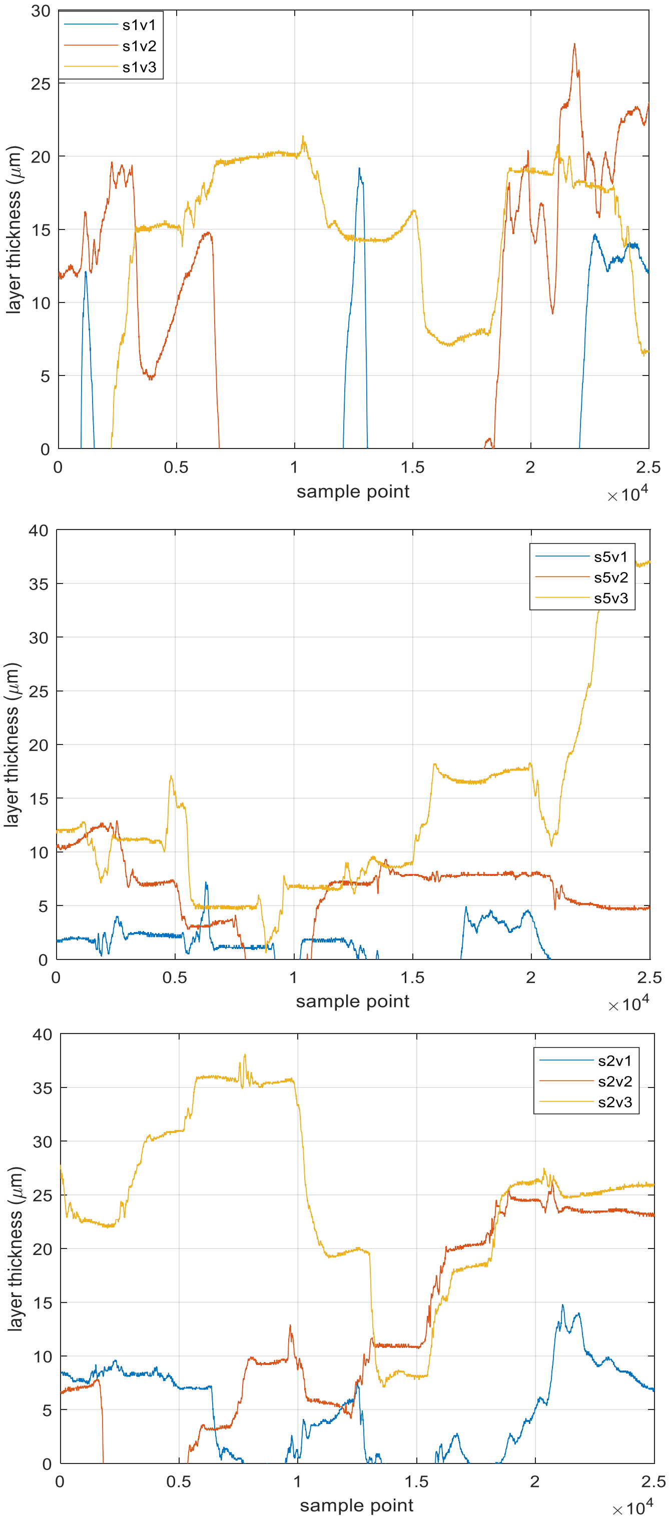

Fig. 26 2-D optical profilometer scans across the inner diameter of the reservoir for each sample (s1v1, s1v2, etc., refer to Table 1). s1, s2, and s5 are methanol, ethanol, and MEK as the solvent, respectively. v1, v2, and v3 are at different solute weight concentrations (Table 1). The reservoir inner diameter is 3.2 mm.

The 2-D optical profilometer scans identified the layer with the most uniform layer with relatively low standard deviation and continuous thickness while being within the optimal thickness range of 2.5 to 10 µm based on the Russo et al. numerical method.[10] In Fig. 26, the gaps in the scans are where there are gaps in the coatings, meaning a noncontinuous layer. The coating formed from the s5v2 droplet satisfied all of those listed conditions.

Crystal uniformity was measured with a microscope camera at a magnification of approximately 800×. Crystals and grain sizes were measured at five locations within the SU-8 reservoir: one center point and four points at the perimeter of the coating. The crystal features for all samples were mostly the same relative to shape and dimensions at the five locations. With MEK as the solvent, the needlelike crystal features were 1 or 2 microns wide and a few microns in length long, whereas the rest of the samples using ethanol and methanol were 10s of microns long and a few microns wide. In general, the crystal features with MEK as the solvent were much smaller at all three solute wt/wt %, which allowed the coating to be more continuous with less gaps and uniform shown with the optical profilometer scans. Figure 27 shows the microscope images of different crystal formations.

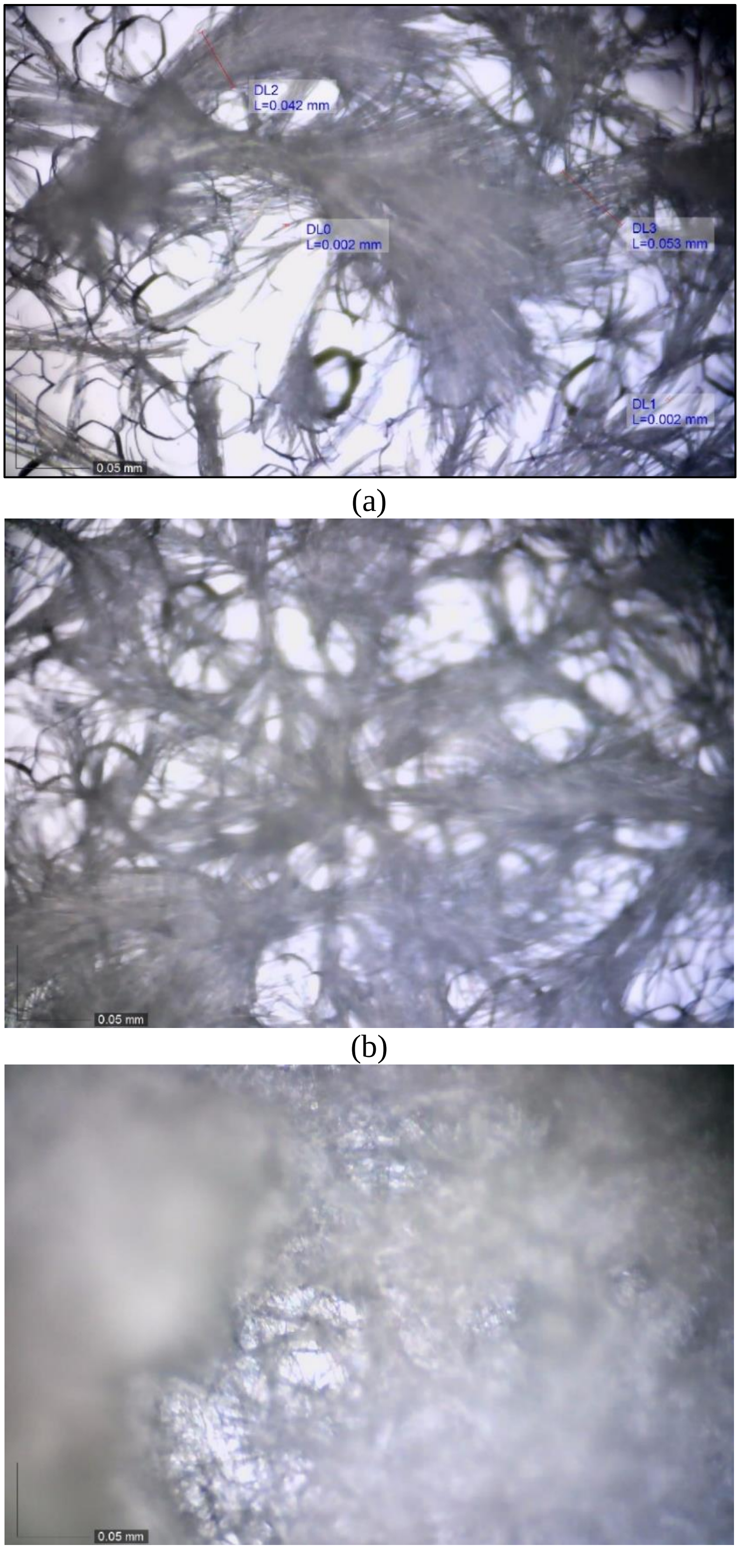

(a)

(b)

(c)

Fig. 27 Microscope image of the C2 crystallization completion: a) s1v1, b) s2v1, and c) s5v2 (refer to Table 1) at a magnification of approximately 800×

Based on the results, two types of solutions were selected for dispensing on HARMST surfaces. The solution with 14 wt/wt % of solute using MEK, s5v2 in Fig. 27c, was the first candidate because of its 2-D surface uniformity with the most continuous layer, low layer thickness relative to other coatings, and the smallest crystal features. The second candidate was the solution with approximately 6 wt/wt % of solute using ethanol, s2v1 in Fig. 27b. This candidate was selected as a comparison on how crystal feature sizes affect the coating quality and overall surface uniformity when deposited on HARMST surfaces. In addition, its surface uniformity with an approximate thickness less than 10 µm for most of the scan is second in comparison to the first candidate.

9. Dispensing and Crystallization on HARMSTs

For each of the sets of pictures in this section, the left picture is a MATLAB processed version where the droplet and crystallization were isolated (Fig. 28a). This was done by taking the first frame of the video before the droplet was dispensed and subtracting it from each of the following frames after the droplet was dispensed. The difference between the two images would be showing the evaporative crystallization as it moves through the rectangular pillar array. The purpose of doing this is to make it easier to perform calculations about the surface area of the crystallization as well. The right picture is a still image from the corresponding frame of the video (Fig. 28b).

Again, the transparency of the liquid caused issues in terms of processing. From an initial viewing, it seemed that the crystallization process changed the color of the rectangular pillar array to a slightly different tint of yellow. This was beneficial to the MATLAB program since it was easily able to figure out the difference between the first frame and the current frame. The MATLAB program had a very easy time discerning the droplet on the planar side, which is the black portion of the image. Notice how the program is able to identify the planar crystallization as one big white contained area. Having the MATLAB program be able to have the desired areas be entirely white would be the goal to achieve for the rectangular pillar side in the future, as it is easier to perform calculations and analysis when this occurs. This would either be done by improving the program and its detention method or dispensing on a different type of surface that responds more drastically when the droplet spreads throughout it so it is easier to analyze.

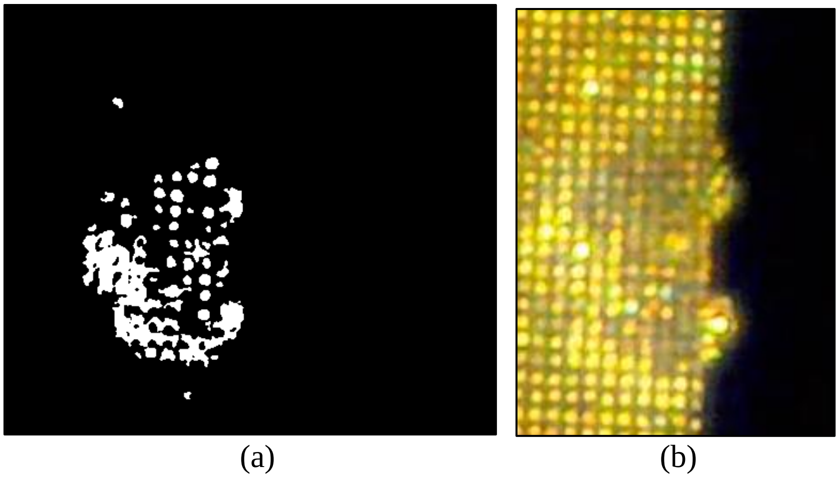
(a) (b)

Fig. 28 **Initial crystallization of s5v2 deposited on Si rectangular pillar and planar surface: a) MATLAB VCA processed image and b) actual microscope image**

9.1 MEK-Based Solution Crystallization

Figure 28 shows the start of the crystallization process after the droplet dispensed and flowed over the surface and in between the microstructure gaps. As a reference, each square in the picture on the right is 5 µm by 5 µm in length and width. Also, it is important to notice that the crystallization is slightly faster on the left with the rectangular pillar array than with the planar surface on the right.

After 1 s and 2 s elapsed, the solution spread very rapidly through the rectangular pillar array (Figs. 29 and 30). Its shape took the form of a semicircle on the 3-D pillar surface. The semicircle had not formed completely on the right side yet, as there is a divot in the middle.

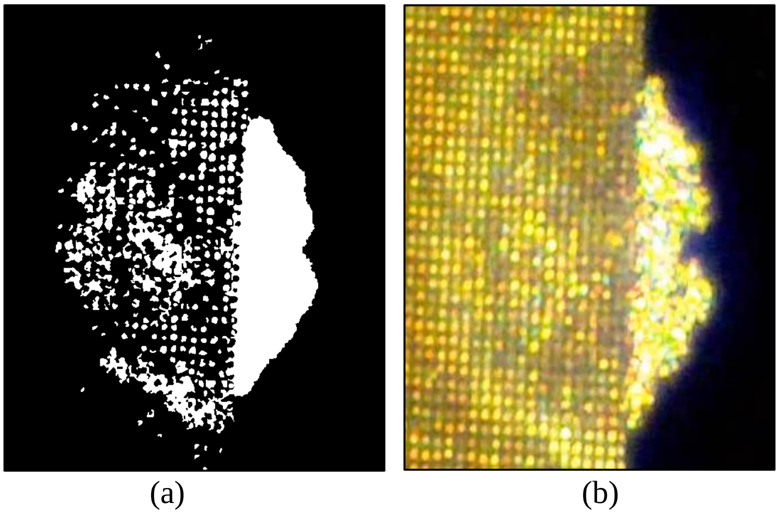
(a) (b)

Fig. 29 **Crystallization of s5v2 after deposited on Si rectangular pillar and planar surface (1 s elapsed): a) MATLAB VCA processed image and b) actual microscope image**

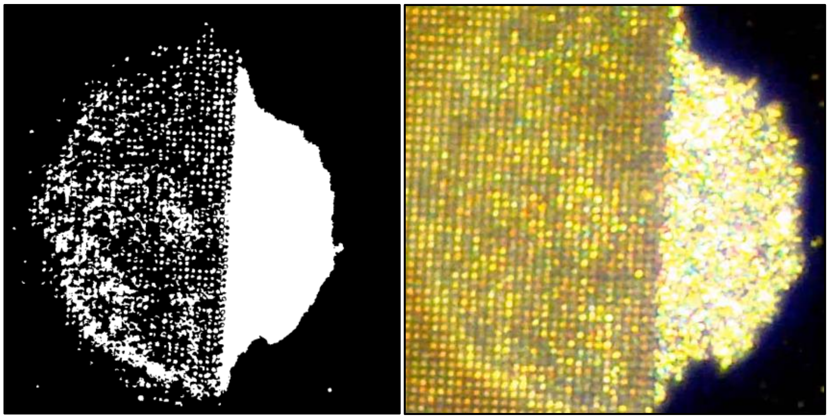

(a) (b)

Fig. 30 Crystallization of s5v2 after deposited on Si rectangular pillar and planar surface (2 s elapsed): a) MATLAB VCA processed image and b) actual microscope image

After 5 s elapsed, the MEK solvent was completely evaporated out and the crystallization over and in between the rectangular pillar array structures was completed crystallized while the planar surface was still in the middle of the crystallization process (Fig. 31). It would take close to 10 s in total for the crystallization to completely cover the planar region. It would be desired for the entirety of the left side (Fig. 31a) to be white as the crystallization process had completed and the entirety of the surface had been covered. The fact that there is a considerable amount of black rendering by the VCA makes the analysis of the surface area calculations more difficult.

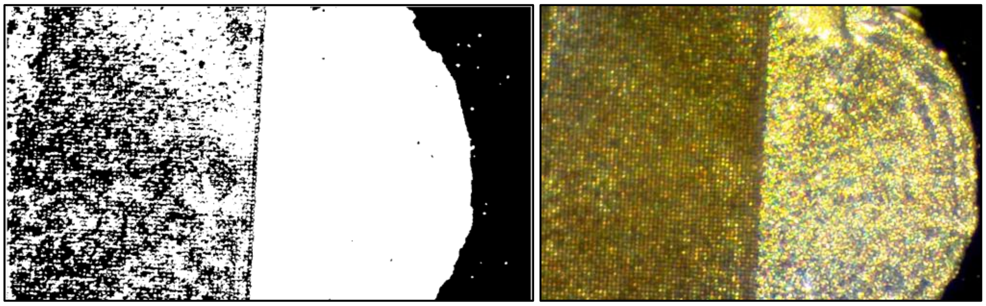

(a) (b)

Fig. 31 Crystallization of s5v2 after being deposited on the Si rectangular pillar and planar surface (5 s elapsed): a) MATLAB VCA processed image and b) actual microscope image

9.2 Ethanol-Based Solution Crystallization

Figure 32 shows a zoomed-in screenshot of the beginning of the s2v1 crystallization after it was deposited on the Si rectangular pillar array. It is at the top of the rectangular pillar array structure, as this was where the crystallization started. Fig. 32a shows the MATLAB VCA processed image of what the program detected, which was different than the original image. The program is not yet optimized as the semicircle seen on the right image is not entirely filled out on the left. The planar region was not analyzed this time because the crystallization process was too slow. After a couple of minutes, only a very small portion of the region had crystallized.

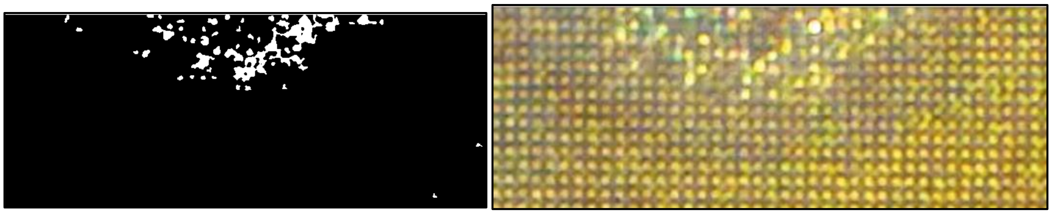
(a) (b)

Fig. 32 Initial crystallization of s2v2 after being deposited on the Si rectangular pillar and planar surface (1 s elapsed): a) MATLAB VCA processed image and b) actual microscope image

After 15 s, it can be seen that the crystallization is coming from the right side of the frame as well as the top (Fig. 33). Calculating the area at this frame involved treating the top and side as semi-ellipses and finding their major and minor axes.

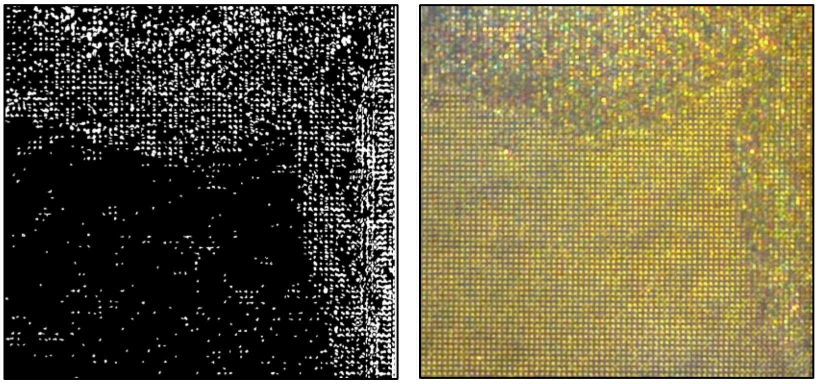
(a) (b)

Fig. 33 Crystallization of s2v1 after being deposited on the Si rectangular pillar and planar surface (15 s elapsed): a) MATLAB VCA processed image and b) actual microscope image

After 30 s, a grain boundary can be seen forming between the top and right regions (Fig. 34). The boundary goes from the middle all the way to the top right. In addition, crystallization from the bottom left is starting and is moving slowly towards the top/right combination.

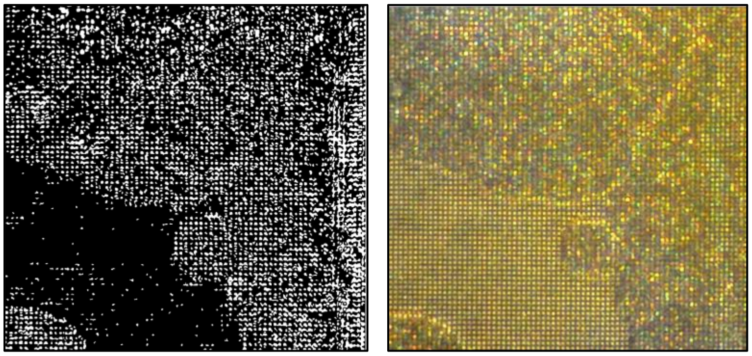

(a) (b)

Fig. 34 Crystallization of s2v1 after being deposited on the Si rectangular pillar and planar surface (30 s elapsed): a) MATLAB VCA processed image and b) actual microscope image

The process finished after 68 s with the grain boundary clearly seen on the right image (Fig. 35b). It starts at the top right and goes down to the bottom left, while branching out a couple of times. This type of grain boundary is unique, since it was not seen when dispensing the ethanol-based solution. The MATLAB VCA processed image struggled to see this grain boundary as clearly. This does not cause an issue, as the grain boundary does not affect the surface area calculations.

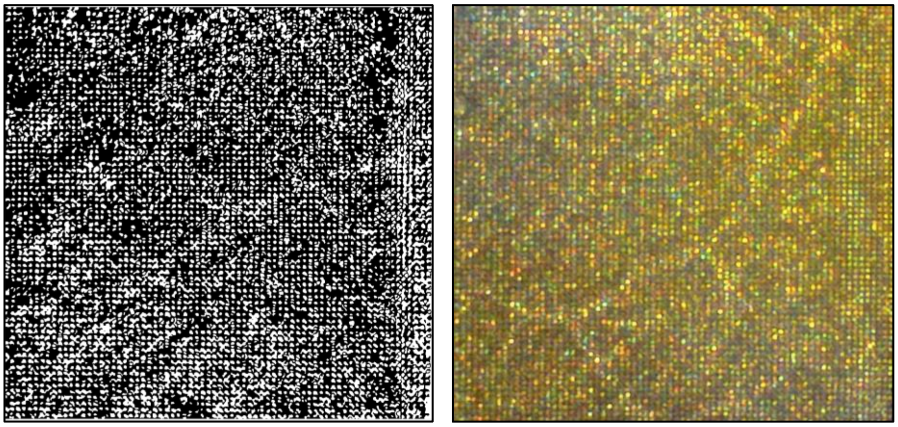

(a) (b)

Fig. 35 Crystallization completion of s2v1 after being deposited on the Si rectangular pillar and planar surface (68 s elapsed): a) MATLAB VCA processed image and b) actual microscope image

10. Rectangular Pillar Array Crystallization Growth Rates

10.1 Sample Calculation Overview

The white area in Fig. 35 indicates crystallization. The white area in Fig. 36 can be split into two semi-elliptical regions. This is an approximation since the top semiellipse is not completed in this frame. It is finished outside the frame of the video, so the area calculated is going to be a slight underestimation. The major/minor axis are calculated from finding the points on the picture that best define the major/minor axis. Then the area can be calculated in pixel^2. Finally, this value can be converted to μm^2. The distance formula and area of ellipse formulas were required for the pixel to micron area conversion given in Eqs. 1 and 2,

$$d = \sqrt{(x_2 - x_1)^2 + (y_2 - y_1)^2} \tag{1}$$

$$A = \pi * a * b, \tag{2}$$

where (x_1, y_1) and (x_2, y_2) are coordinates and a and b are the major/minor axis respectively as most regions are elliptical rather than circular. For the pixel to micron conversion, each yellow square in the original video is 5 × 5 µm in length and width. The length of the microstructure region is 60 squares in the video, meaning it represents an area of 300 microns. The pixel length dimension is 950 pixels, which means there are 3.1 pixels for every micron.

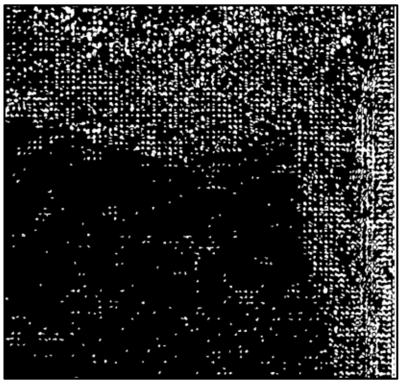

Fig. 36 Crystallization screenshot of s2v1 used for crystallization rate calculation

10.2 MEK-Based Solution Crystallization Rate

Table 6 compares the rate of crystallization over the two different types of structures: HARMST and planar. It should be noted that in the video the area for the two different regions was not the same. The maximum area of the HARMST region was 100,000 µm^2 while it was 112,500 µm^2 for the planar region. The clarification is important since it does not appear that the planar region grew more within the same timeframe. The crystallization ran out of space to spread on the HARMST region much faster. Figure 37 clarifies this point further.

Table 6 **s5v2 crystallization over HARMST and planar surfaces as time elapsed**

Time elapsed (seconds)	Crystallization area formed over HARMST surface (μm^2)	Crystallization area formed over planar surface (μm^2)
1	12,900	4,100
2	34,000	10,200
3	58,000	32,500
4	80,000	42,000
5	91,000	56,000
10	100,000	112,500

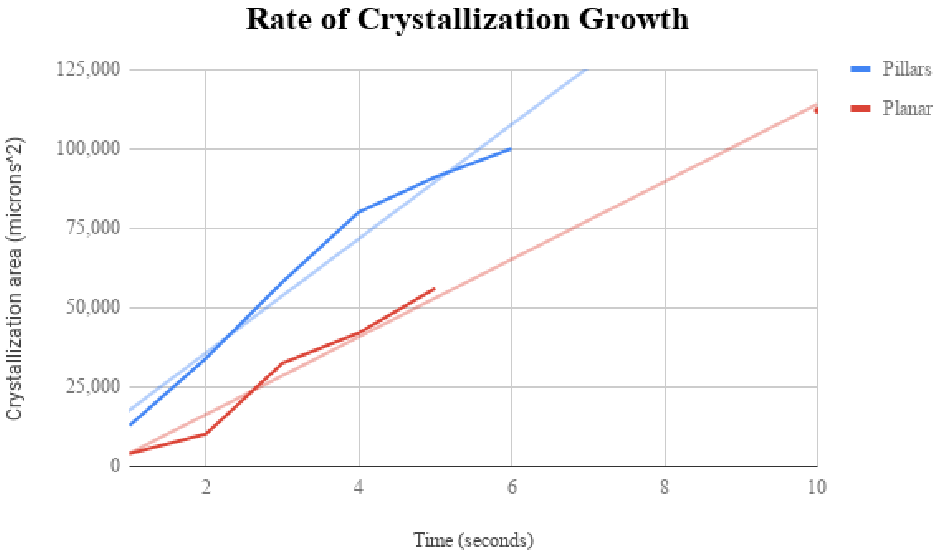

Fig. 37 **s5v2 crystallization area as a function of elapsed time with trendlines that are a fainter shade**

There is a trendline for both the pillar and planar region (Fig. 37). It shows that if the pillar region were larger, it would have achieved a surface area coverage of 125,000 µm^2 at 7 s, which is 3 s faster than it took for the planar region to cover the same amount of surface area. According to the trendline, the HARMST region grew at approximately 17,800 µm^2 per second. The planar region grew at approximately 11,200 µm^2 per second. The crystallization rate is faster with the HARMST region because of the surface area difference. The evaporative crystallization rate is directly related to surface area. The evaporative crystallization was faster with the HARMST region because the surface area was greater than the planar region.[12]

Figures 38 and 39 are used to indicate how the rate of crystallization growth changes over time on rectangular pillar array and planar surfaces. The rate of crystallization keeps increasing up to around 3 s. Between each interval up to 3 s, the crystallization occurred faster with every second. The crystallization slowed down because the viewing space on the microscope camera was running out on the screen for the crystallization growth. This fast and accelerated initial crystallization makes MEK the primary solvent choice for the tritiated nitroxide nuclear battery as it goes through the process very rapidly when compared to ethanol. The whole process is done within 6 s on the rectangular pillar array, which is about 10 s before approximately 50% of the surface area is covered after the solution was dispensed.

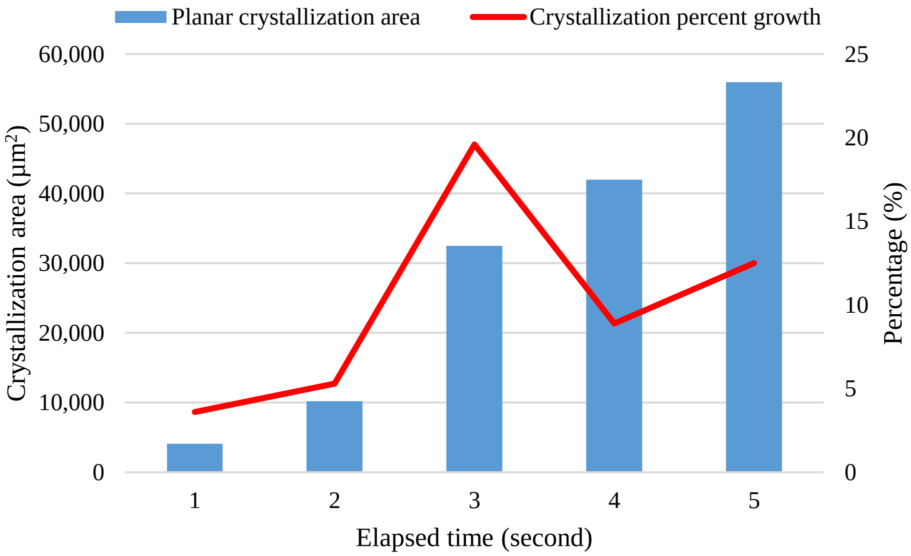

Fig. 38 s5v2 crystallization area and growth percentage as function of elapsed time on planar surface

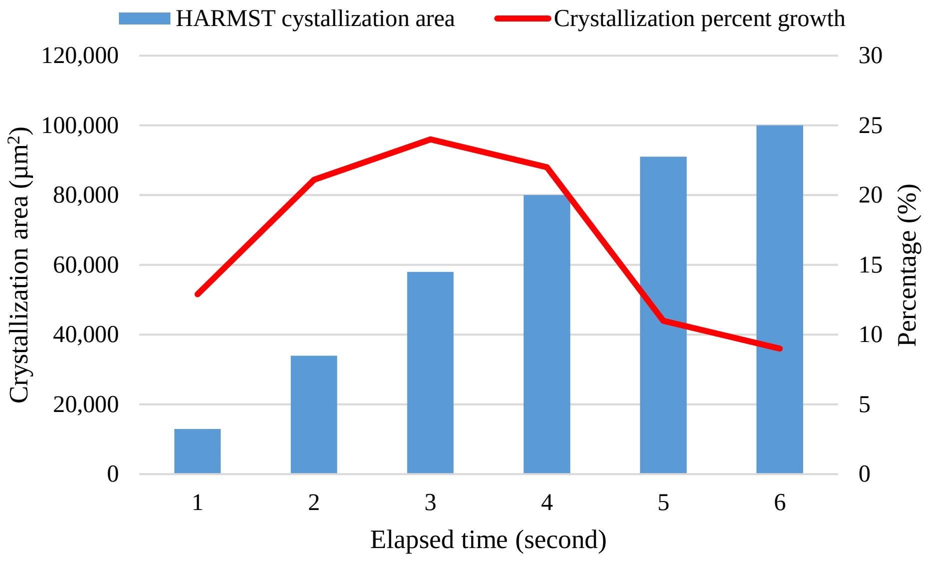

Fig. 39 s5v2 crystallization area and growth percentage as function of elapsed time on HARMST surface

10.3 Ethanol-Based Solution Crystallization Rate

There is no measurement or calculation for the planar surface with the ethanol-based solution. The growth rate was simply too slow to measure. The crystallization growth rate was a magnitude less than the HARMST structure, which is already a magnitude less than MEK-based solution crystallization on the HARMST surface. The reason the last interval was at 68 s is because the video stopped at that time and the evaporation had completed. The maximum surface area possible was 142,500 µm^2 (Table 7).

Table 7 s2v1 crystallization over HARMST surface as time elapsed

Time elapsed (seconds)	Crystallization formed over HARMST surface (μm^2)	Crystallization percent growth
15	66,000	46%
30	108,000	29%
45	126,000	12.6%
60	140,000	9.8%
68	142,500	1.7%

The red line corresponds with the percent increase per interval and corresponds with the right scale. The trend is that the percent increase in crystallization is lessening as time goes on. The crystallization process is slowing down the entire time, which is much different than the process for MEK-based solution. Therefore, the crystallization process of the s2v1 can be characterized by an initial burst followed by a continuously slowing process (Fig. 40).

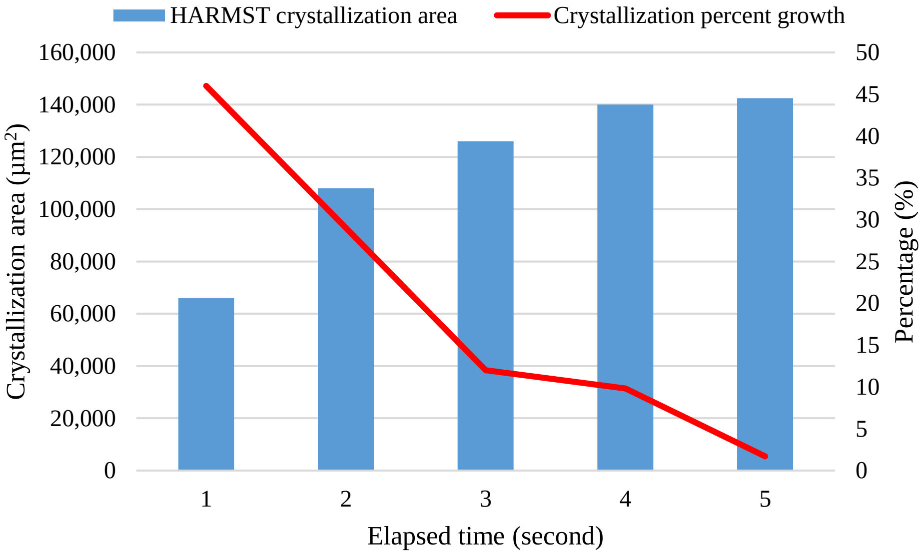

Fig. 40 s2v1 crystallization area and growth percentage as function of elapsed time on HARMST surface

11. Profilometer and Microscope Measurements for Surface Topography and Crystal Uniformity on Rectangular Pillar Array Surfaces

After the completion of the MATLAB VCA with the rectangular pillar arrays, the surface topography, approximate thickness and bulk density, and crystal uniformity were measured by calibrated instruments. This process was identical to the planar surface analysis with further analysis. This additional analysis step produced the surface topography of C2 deposition on HARMST. The larger surface area of the sample allowed seven scans across the sample surface rather than only one scan across the sample's diameter, as described in Section 8.2. The optical profilometer data was smoothed using Savitzky-Golay filtering, which is often used with frequency and spectroscopic data.[13] Biharmonic spline interpolation was used as the surface topographic curve fit for the seven scans. Biharmonic spline interpolation is a type of bicubic interpolation of irregularly spaced 2-D data points often used as topographic curve fit for GEOSAT and SEASAT altimeter data.[14] Figures 41 and 42 show the surface topography and contour plots using this curve fit process. The two HARMST samples used the two solutions selected from the planar analysis described in Section 8.2.

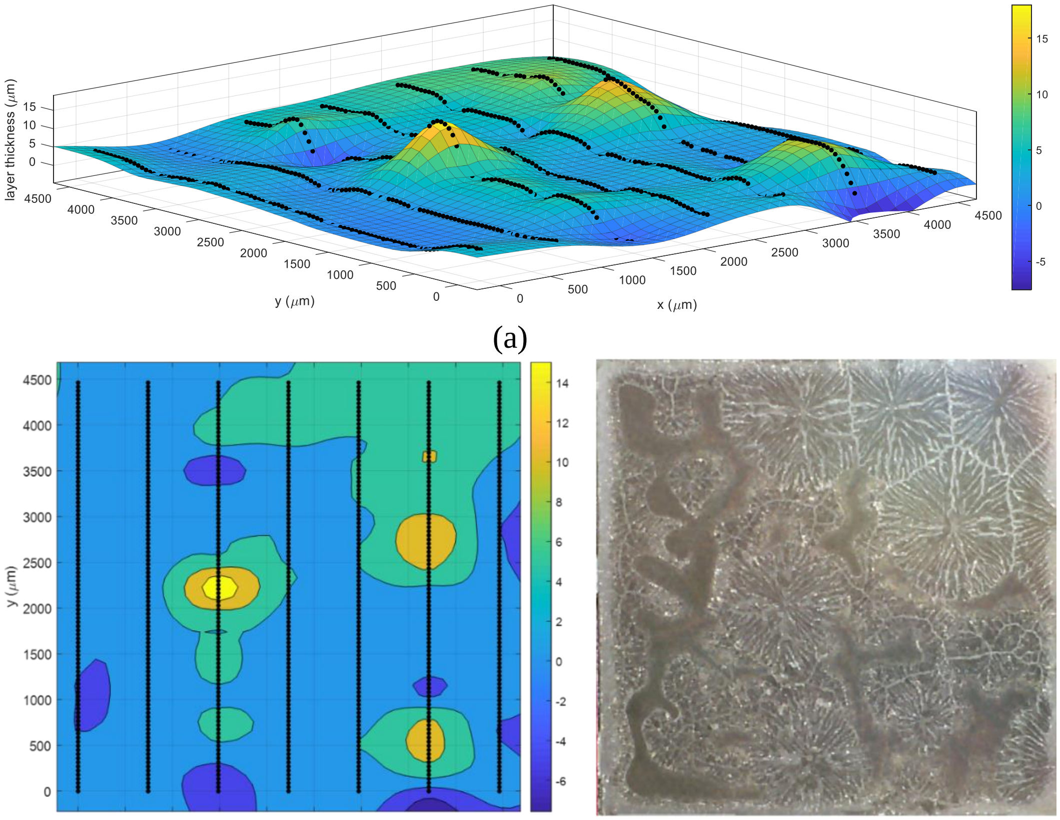

(a)

(b)

(c)

Fig. 41 C2 crystallized on Si rectangular pillar array using the s5v2 solution: a) surface topography, b) contour plot, and c) microscope image. The colorbar units are microns. The black dots shown in (a) and (b) are the data points from the 2-D profilometer scan. Biharmonic spline interpolation produced the surface curve fit.

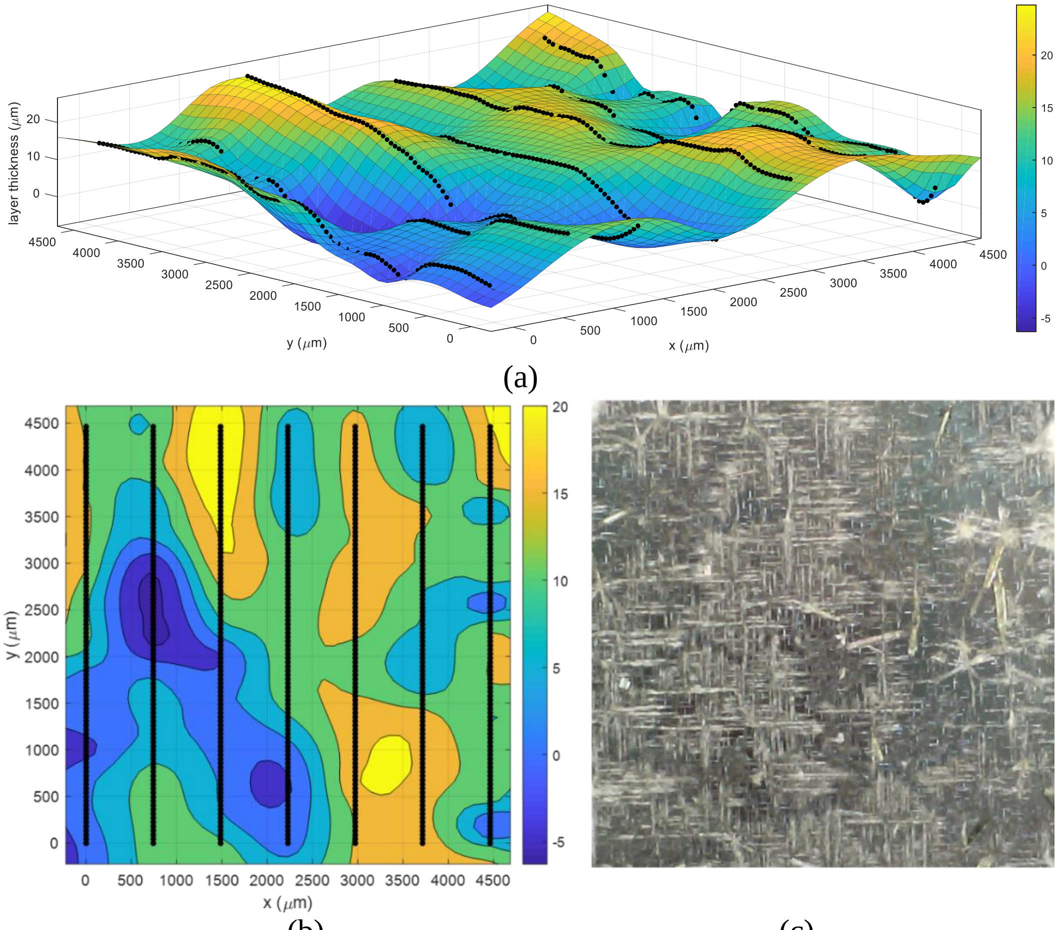

(a)

(b) (c)

Fig. 42 C2 crystallized on Si rectangular pillar array using the s2v1 solution: a) surface topography, b) contour plot, and c) microscope image. The colorbar units are microns. The black dots shown in (a) and (b) are the data points from the 2-D profilometer scan. Biharmonic spline interpolation produced the surface curve fit.

The solution with approximately 14 wt/wt % of solute using MEK, called s5v2, produced a more uniform surface topography than the solution with approximately 6 wt/wt % of solute using ethanol, called s2v1. Tables 8 and 9 show area percentages of different thickness ranges of surface topography with s5v2 and s2v1. For s5v2, a majority of the layer thickness was between 0 to 5 µm. There were only four peaks where the layer thickness was between 10 to 15 µm. As previously stated, layer thicknesses between 2.5 to 10 µm will maximize the bidirectional beta (β^-)-flux surface power density.[10] The surface topography curve fit matched well with the microscope image shown in Fig. 41a and b. The peak and higher plateau area were where the lamellar branching spherulites were located. The low areas were where the amorphous regions were located. These are the areas between lamella spherulites. The approximate bulk density of the C2 layer on planar and HARMST surfaces is 0.6417 ± 0.12 g/cm^3 and 0.25 ± 0.022 g/cm^3, respectively.

The approximate bulk density was based on the weighted area percentage of thickness from the surface topography curve fit. For the surface topography with s2v1, there were more areas in the shape of ridges with layer thickness between 15 to 20 µm. A majority of the surface topography was greater than or equal to 10 µm. In addition, there were larger areas where the layer thicknesses were between 0 to –5 µm, meaning that the rectangular pillar's gaps were partially filled. This was also measured in the s5v2 but with a smaller area. The seven profilometer scans were averaged for s5v2 and s2v1 samples shown in Fig. 43. As another representation of the surface topography relative uniformity, the s5v2 sample's average layer thickness and standard error are lower than the s2v1 sample (Fig. 43).

Table 8 C2 layer thickness area percentage using s5v2 solution. Layer thickness area percentage is calculated from contour plot (Fig. 41b).

Layer thickness range (µm)	Area percentage
0 to 4	68.8%
4 to 6	26.6%
10 to 12	2.98%
14 to 15	0.32%
-4 to –6	0.77%
–6 to –8	0.53%

Table 9 C2 layer thickness area percentage using s2v1 solution. Layer thickness area percentage is calculated from contour plot (Fig. 42b).

Layer thickness range (µm)	Area percentage
15 to 17.5	20.9%
0 to –5	4.25%
5 to 7.5	21.0%
17.5 to 20	4.32%
–5 to –7.5	1.33%
0 to 5	13.7%
10 to 12.5	34.5%

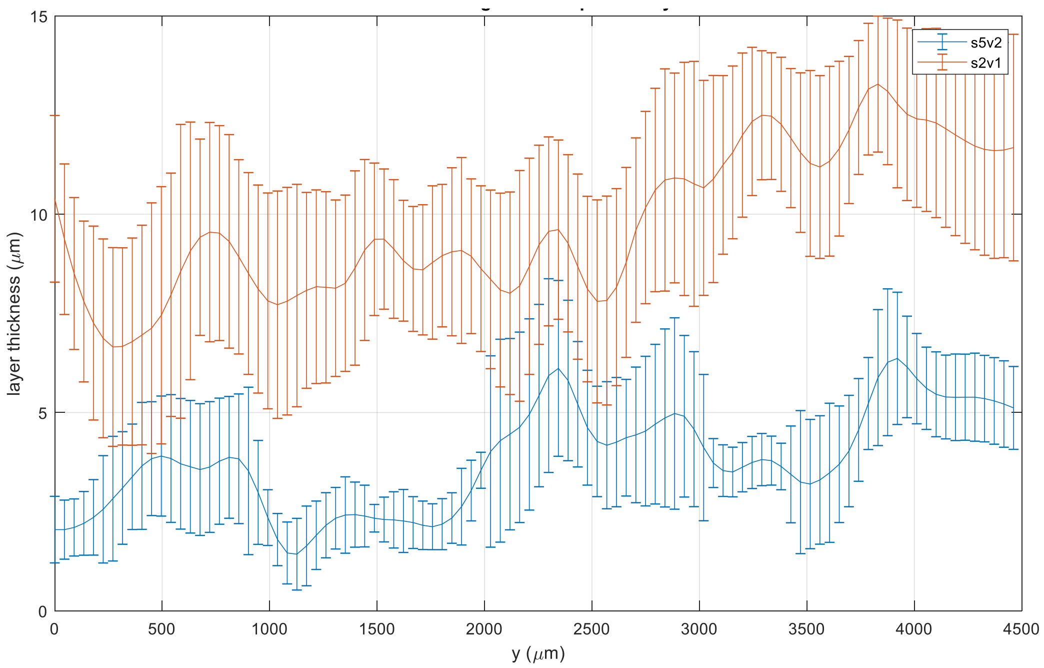

Fig. 43 Average 2-D surface plot of C2 deposited on HARMST using s5v2 and s2v1. The error bars are the standard error between the individual 2-D scans across the surface.

Crystal uniformity, similar to the planar analysis, was observed with a microscope camera at a magnification of approximately 42× and 800×. Figures 44 and 45 show images of the samples after evaporative crystallization had completed. As it was expected based on previous planar results, the s5v2 sample displayed more crystal uniformity than the s2v1 sample. For the s5v2 sample, there were lamellar spherulites at different grain sizes' amorphous regions between them. This was also true when observing the crystal formation surrounding the HARMST region. The tops of the rectangular pillars were slightly visible but distorted because of the nitroxide C2 coating being partially translucent. For the s2v1, the crystal structures were nearly identical to the structures forming on a planar surface. The needlelike crystals were hundreds of microns long and a few microns wide. Much of the rectangular array was exposed displaying the lack of C2 deposition over the top of the HARMST. The crystal features were just too large to completely fill the gaps between the rectangular pillars. Based on both analyses' results, it was decided that s5v2 is the optimal solution for depositing nitroxide C2 on planar and HARMST surfaces.

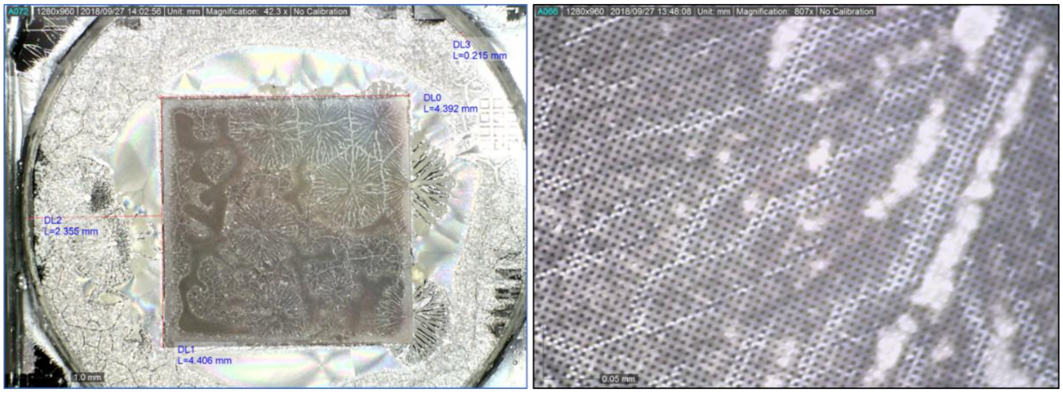

(a) (b)

Fig. 44 Microscope images of C2 crystallized on HARMST surface using the s5v2 solution at magnification of approximately a) 40× and b) 800×

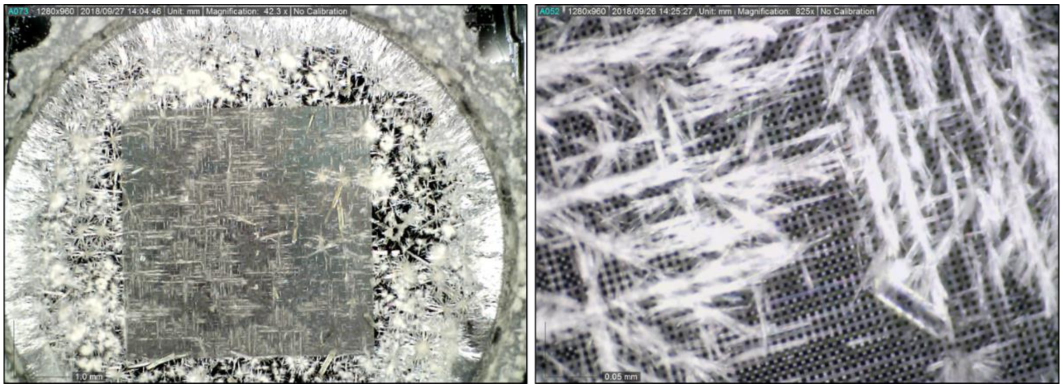

(a) (b)

Fig. 45 Microscope images of C2 crystallized on HARMST surface using the s5v2 solution at magnification of approximately a) 40× and b) 800×

12. Surface Area Crystallization Rates with GaN Ridge Arrays

12.1 Introduction

Surface uniformity and layer thickness using the optical profilometer were not measured because the uGaN is translucent. A zero point could not be established because the red laser would irradiate through the wafer. Only MATLAB VCA was used to analyze the evaporative crystallization growth along with the microscope camera images to measure the crystal and grain dimensions after the evaporative crystallization. The same VCA process used with the crystallization over Si rectangular pillar arrays was implemented for the uGaN ridge arrays. First, the time for crystallization process was measured. This was subjectively determined by when it was unable to be seen that the crystallization process was continuing or when the camera shifted away to other parts of the surface. Each graph contains two plots. The blue line in every plot is the rate of crystallization of the 3-D microstructure, while the orange line is the rate of crystallization for the planar surface. The rate of crystallization is measured by the total surface area of crystallization over the possible surface area for that region. Representing this as a percentage created a normalization since the amount of area differed per region. The difference in area per region was due to the placement of the camera.

The reason that this set of plots are made up of continuous graphs compared to HARMST pillar structures has to do with the identification quality of the crystals in the MATLAB VCA. In the figures from Section 10, there were always black regions even if the entire area was covered by C2 crystals since the program had difficulty discerning if an area had actually crystallized or not (because the color change was very slight). In contrast, the program was effectively able to determine and create solid crystallization areas for the uGaN surfaces. A comparison of the two renderings is shown in Fig. 46.

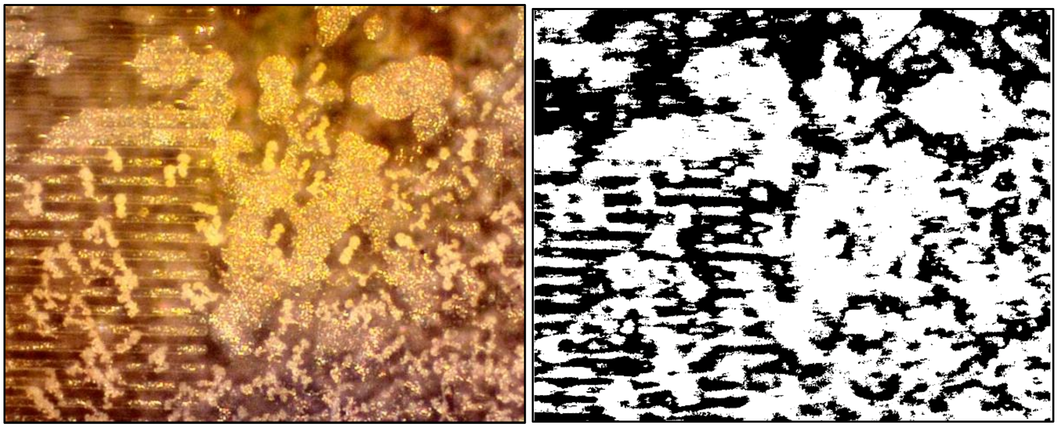
(a) (b)

Fig. 46 Evaporative crystallization over uGaN ridge array (*w* = 15 µm and *a* = 20 µm): a) microscope image and b) MATLAB VCA processed image. The black region of (b) is where the planar and HARMST surface have not crystallized. The white region is where the evaporative crystallization has completed. The crystallization occurs immediately on top of the ridges and planar surface. The ridge gaps are the last to crystallize. This trend was repeated with the other ridge array dimensions.

Most of the plots presented in this section follow the same logistical curve. The main difference between the uGaN surface and the Si surface is the fact that the spread of crystallization was actually faster over the planar surface when compared to the HARMST (3-D) surface. This difference, while originally unexpected, can be explained due to a difference in the experimental setup between the two surfaces. Reservoirs were not used. In addition, the surface area of the planar region was larger than the HARMST region. The HARMST features were 3× wider than the rectangular pillars with gaps at least 4× wider. In general, there was more planar surface area than HARMST surface area. A larger surface area leads to a faster evaporative crystallization rate.[12]

12.2 uGaN ridge array: 15 µm width (w) and 20 µm gap (a)

In Fig. 47, the x-axis indicates the frame number in the video. The plot starts at frame 100 because that is when the droplet is dispensed on the GaN surface. Once dispensed, the crystallization begins to form faster on the HARMST surface. 200 frames into the evaporative crystallization, the crystallization area for the planar surface overtakes the HARMST surface and continues this for the rest of the video. By the end of the video, the planar surface is coated with a larger crystallization area than crystallization over the HARMST surface.

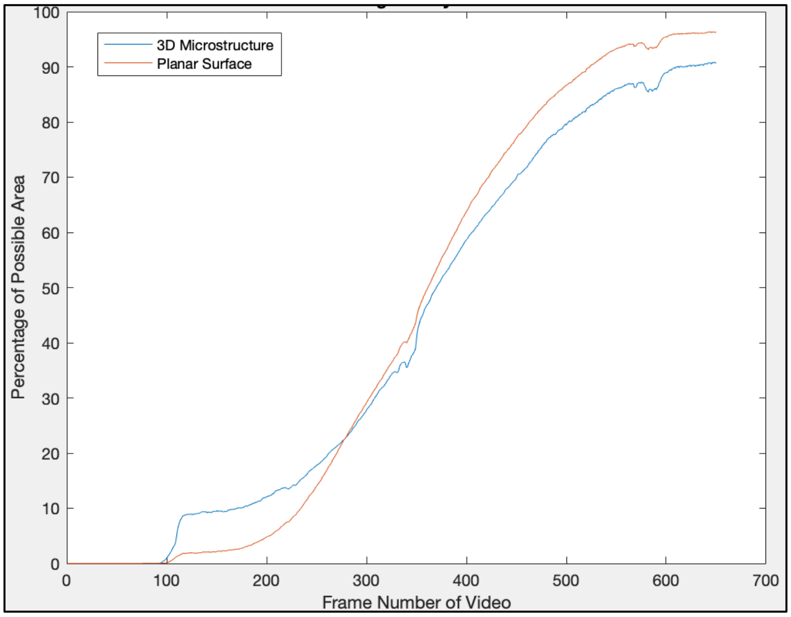

Fig. 47 Crystallization of uGaN ridge array and planar surface as function of video frame number. The solution was s5v2, and the ridge dimensions were w = 15 µm and a = 20 µm.

12.3 uGaN ridge array: 15 µm width (w) and 30 µm gap (a)

With the 15 µm width (w) and 30 µm feature gap (a) uGaN ridge array, the planar surface crystallization had the familiar logistical growth pattern to it (Fig. 48). However, the plot differed from the previous plot with the crystallization percentage of the HARMST surface. First, there was no initial spike of crystallization as found with the other uGaN ridge array configurations. The plot for the 3-D microstructure also appears to be more parabolic, $f(x) = ax^2 \ with \ a < 1$, as seen by its wide shape and slow crystallization growth. Another interesting trend is that it only reached around 50% of the total possible area. For most of the plots that ended up with a logistic curve, the final area percentage was around 95% by the time the video had finished.

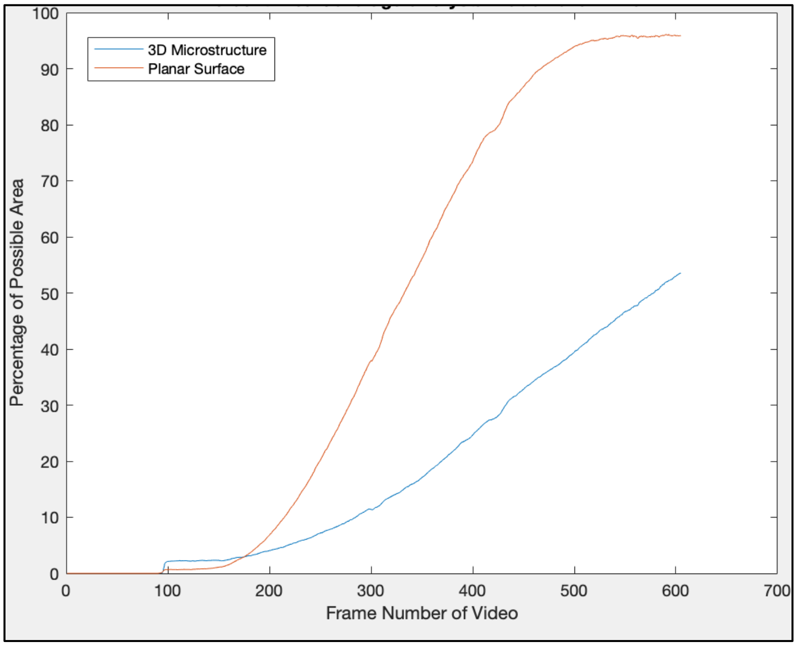

Fig. 48 Crystallization of uGaN ridge array and planar surface as function of video frame number. The solution was s5v2, and the ridge dimensions were *w* = 15 µm and *a* = 30 µm.

13. Conclusion

The evaluation of solutions with different solvents at various solute wt/wt % identified the optimal combination to use for deposited tritiated nitroxide on planar and HARMST surfaces. The parametric study involved VCA as well as calibrated instruments to generate quantitative and qualitative results. By relating and comparing the results for each sample, the evidence was clear that one type of solution, s5v2, produced satisfactory quantitative and qualitative results. The solvent type is MEK; the solute weight concentration is 14 wt/wt %. The planar and HARMST surface uniformity was relatively uniform with layer thickness fitting within the thickness range that is considered optimal when using the tritiated nitroxide as a power source. Identifying the optimal solution from this parametric study was the primary goal.

The secondary goal was accomplished by designing a method to deposit or dispense nitroxides on planar and HARMST surfaces and characterizing the crystallization behavior, surfaces, and crystals. The importance of using a simple manufacturing process is threefold: cost, time, and safety. Two- to three-step synthesis, depending on nitroxide type, one-step tritiation, and depositing at SATP with just micropipette, lowers the overall cost of the nuclear battery manufacturing process.

Also, from evidence shown in this report, the deposition method does not need to completely change when switching from planar to HARMST betavoltaic cells. A betavoltaic nuclear battery will most likely involve hundreds of betavoltaic cell and radioisotope source (tritiated nitroxide) stacked layers using a stacking configuration to construct a milliwatt power source.[15] Evaporative crystallization time needs to be minimized to reduce the overall assembly time of the power source. In addition, the sooner the crystallization is completed, the faster the user can apply potting or a type of encapsulate to reduce the chances of tritium exposure if leakage does occur.

Characterizing the nitroxide C2 coatings involved noncontact measurement techniques. Contact methods such as a stylus profilometer or atomic force microscope could potentially distort or disrupt the coating surface, which is held together by van der Waals force only. MATLAB VCA was implemented to measure rate of crystallization and surface uniformity. An effort to observe crystallization moving along the HARMST feature gaps was attempted, but the changes in lighting during crystallization produced too much variability for any conclusive results. We would still require a noncontact profilometer to measure the surface topography, which would identify if the C2 coating filled in the gaps. The VCA results were confirmed accurate with the use of calibrated instruments: optical profilometer and microscope camera. There was no discrepancy with each method. This overall agreement was demonstrated with the HARMST results. There were minor discrepancies between the crystallization rates of the rectangular pillars and ridges. Crystallization rates were faster with the Si's HARMST surfaces compared to the uGaN's HARMST surfaces. Experimental setup and surface area difference were the major factors for this opposite trend. For the rectangular pillar array, a reservoir contained the solution during evaporative crystallization and the HARMST surface area was significantly greater than the planar surface area. This was not case relative to both factors for the uGaN ridge array. Samples using s5v2 as the solution displayed the best metrics, relative surface topography and crystal uniformity, and optimal thickness range calculated in Russo et al.[10], compared to other solutions tested in this experiment. Finally, these results did not change when using a different HARMST type demonstrated with the uGaN ridge arrays. VCA and crystal uniformity results showed similar traits with the Si rectangular pillar arrays. The crystal shapes were very similar when compared to the Si rectangular pillar arrays even though the aspect ratios were very different. Most importantly, the C2 coatings were able to fill in the gaps between both types of HARMST features: pillars and ridges.

14. References

1. Romer M. Ragone plot comparison of radioisotope cells and the direct sodium borohydride/hydrogen peroxide fuel cell with chemical batteries. IEEE Trans Energy Convers. 2008;23(1):171–178.

2. Carroll JJ. Nuclear metastables for energy and power: status and challenges. In: Shaffer EC, Zheleva TS, editors. Innovations in Army Energy and Power Materials Technologies. Millersville (PA): Materials Research Forum LLC; 2018. p. 290–305.

3. Bower KE, Barbanel YA, Shreter YG. Polymers, phosphors, and voltaics for radioisotope microbatteries. Boca Raton (FL): CRC Press; 2002.

4. Kavetsky AG, Nekhoroshkov SN, Meleshkov SP, Kaminski YL, Akulov GP. Radioactive materials, ionizing radiation sources, and radioluminescent light sources for nuclear batteries. In: Bower KE, Barbanel YA, Shreter YG, Bohnert GW, editors. Polymers, Phosphors, and Voltaics for Radioisotope Microbatteries. Boca Raton (FL): CRC Press; 2002. p. 6–40.

5. Shpil'rain EE, Yakimovich KA, Mel'nikova TN, Polishchuk AY. Thermophysical properties of lithium hydride, deuteride, and tritide and of their solutions with lithium. New York (NY): American Institute of Physics; 1987.

6. Lee S-K, Son S-H, Kim K, Park J-W, Lim H, Lee J-M, Chung E-S. Development of nuclear micro-battery with solid tritium source. Appl Radiat Isot. 2009;67:1234–1238.

7. Revankar ST, Adams TE. Advances in betavoltaic power sources. J Energy Power Sources. 2014;1(6):321–329.

8. Thomas C, Portnoff S, Spencer MG. High efficiency 4H-SiC betavoltaic power sources using tritium radioisotopes. Appl Phys Lett. 2016;108(1).

9. Russo J, Litz M, Ray II W, Rosen GM, Bigio DI, Fazio R. Development of tritiated nitroxide for nuclear battery. Appl Radiat Isot. 2017;125:66–73.

10. Russo J, Rosen GM, Ray II W, Bigio D, Litz MS, Thomas C, Alam TR, Bayne S, Cho H, Yu J. Demonstration of a tritiated nitroxide nuclear battery. Appl Radiat Isot. Forthcoming 2018.

11. ANL. Human Health Fact Sheet: Tritium (Hydrogen-3); 2001 [accessed 2018 Nov 11]. http://hpschapters.org/northcarolina/NSDS/tritium.pdf.

12. Hipple J. Evaporation and crystallization. Newark (NJ): American Institute of Chemical Engineers; 2017. Chapter 12, Chemical Engineering for Non-Chemical Engineers; p. 203–219.

13. Orfandis SJ. Introduction to signal processing. Englewood Cliffs (NJ): Prentice-Hall; 1996.

14. Sandwell DT. Biharmonic spline interpolation of GEOS-3 and SEASAT altimeter data. Geophys Res Lett. 1987;14(2):139–142.

15. Spencer M, Chandrashekhar M, inventors. High power density betavoltaic battery. United States patent US8487392B2. 2013 July 16.

List of Symbols, Abbreviations, and Acronyms

2-D	2-dimensional
3-D	3-dimensional
C2	Compound 2
DMF	dimethylformamide
DRIE	Deep reactive-ion etching
HARMST	high aspect ratio microstructure technology
LEO	low earth orbital
MEK	methyl ethyl ketone
MPP	maximum power point
RPS	radioisotope power source
SATP	standard ambient temperature and pressure
Si	silicon
STP	standard temperature and pressure
uGaN	undoped GaN
VCA	video content analysis

1 (PDF)	DEFENSE TECHNICAL INFORMATION CTR DTIC OCA
2 (PDF)	DIR ARL IMAL HRA RECORDS MGMT RDRL DCL TECH LIB
1 (PDF)	GOVT PRINTG OFC A MALHOTRA
1 (PDF)	ARL RDRL SED E J RUSSO